Intersatellite calibration of AMSU-A observations for weather and climate applications

Cheng-Zhi Zou[1] and Wenhui Wang[2]

Received 4 May 2011; revised 28 September 2011; accepted 29 September 2011; published 13 December 2011.

[1] Long-term observations from the Advanced Microwave Sounding Unit-A (AMSU-A) onboard polar-orbiting satellites NOAA 15, 16, 17, and 18 and European Meteorological Operational satellite program-A (MetOp-A) were intercalibrated using their overlap observations. Simultaneous nadir overpasses (SNOs) and global ocean mean differences between these satellites were used to characterize calibration errors and to obtain calibration coefficients. Calibration errors were found manifesting themselves as certain scatter or temporal patterns of intersatellite biases, such as well-defined seasonal cycles in the Arctic and Antarctic SNO difference time series or a unique pattern closely correlated to the instrument temperature variability induced by Solar Beta Angle (SBA) variations in global ocean mean difference time series. Analyses of these patterns revealed five different types of biases that need to be removed from existing prelaunch-calibrated AMSU-A observations, which include relatively stable intersatellite biases between most satellite pairs, bias drifts on NOAA 16 and channel 7 of MetOp-A, sun-heating-induced instrument temperature variability in radiances, scene temperature dependency in biases due to inaccurate calibration nonlinearity, and biases due to channel frequency shift from its prelaunch measurement in certain satellite channels. Level-1c time-dependent calibration offsets and nonlinear coefficients were introduced and determined from SNO and global ocean mean temperature regressions to remove or minimize the first four types of biases. Channel frequency shift in NOAA 15 channel 6 was obtained from the radiative transfer model simulation experiments. The new calibration coefficients and channel frequency values have significantly reduced the five different types of biases and resulted in more consistent multisatellite radiance observations for intercalibrated satellite channels. The intercalibrated AMSU-A observations have been merged with its precursor, the intercalibrated microwave sounding unit (MSU), to generate the NOAA/Center for Satellite Applications and Research (STAR) version 2.0 upper-air temperature climate data record (CDR) for climate trend and variability monitoring from 1979 to the present. The intercalibrated AMSU-A radiance data are expected to further improve accuracies of numerical weather prediction and consistencies in climate reanalysis and CDR developments.

Citation: Zou, C.-Z., and W. Wang (2011), Intersatellite calibration of AMSU-A observations for weather and climate applications, *J. Geophys. Res.*, *116*, D23113, doi:10.1029/2011JD016205.

1. Introduction

[2] Accurate satellite instrument calibration is a prerequisite for using satellite data in accurate numerical weather prediction (NWP), reliable climate change monitoring, and consistent reanalysis data assimilations. Satellite calibration involves characterization and removal of instrument errors from many different sources, which include, but are not limited to, instrument calibration nonlinearity [*Mo*, 1995; *Zou et al.*, 2006, 2009], calibration target errors [*Twarog et al.*, 2006], antenna pattern correction [*Mo*, 1999], incident angle effect, and spectral response function errors [*Cao et al.*, 2005]. Some of these calibrations can be conducted in the laboratory testing processes prior to satellite launch. However, once a satellite is in its orbit, new calibration issues may arise and prelaunch-determined calibration parameters may change because of changes in the observation environment from the ground laboratories to deep space, satellite exposures to solar radiation and cosmic rays, instrument degradation, and many other factors. These changes may significantly affect the satellite data quality for their subsequent environmental applications. In meeting the challenges of better use of satellite data in weather and climate applications, postlaunch recalibration and especially intersatellite

[1]Center for Satellite Applications and Research, NESDIS, NOAA, Camp Springs, Maryland, USA.
[2]I. M. Systems Group at Center for Satellite Applications and Research, NESDIS, NOAA, Camp Springs, Maryland, USA.

This paper is not subject to U.S. copyright.
Published in 2011 by the American Geophysical Union.

calibration have recently emerged as an important area of research in reducing satellite biases, harmonizing data quality, and ensuring data consistencies among different satellites [*Goldberg et al.*, 2011]. The simultaneous nadir overpass (SNO) concept proposed by *Cao et al.* [2004] and its associated algorithm to find SNO events provide an effective tool in this area of research, enabling characterizing and even reducing certain types of satellite biases that were difficult to tackle before.

[3] The purpose of this study is to intercalibrate the long-term observations from the Advanced Microwave Sounding Unit-A (AMSU-A) onboard NOAA, European Meteorological Operational satellite program-A (MetOp-A, simply referred to as MetOp-A later), and NASA EOS-Aqua (simply referred to as Aqua later) polar-orbiting satellites using their SNOs and global ocean mean temperatures. This is a follow-on effort to the intersatellite calibration of microwave sounding unit (MSU) onboard historical NOAA satellite series in our previous studies [*Zou et al.*, 2006, 2009; *Zou and Wang*, 2010], aiming at the development of satellite microwave-based upper-air temperature climate data record (CDR) for climate trend monitoring and investigations.

[4] The MSU and AMSU-A instruments were designed to measure the atmospheric temperature profiles under all weather conditions, excluding precipitation. The MSU observations covered the period from 1979 to 2007 onboard NOAA TIROS-N through NOAA 14, making temperature measurements from the surface to the lower stratosphere. Starting from 1998 to the present, AMSU-A onboard NOAA-KLM and their follow-on satellite series have replaced MSU. As a successor to MSU, AMSU-A extends its observation to the upper stratosphere from the surface with improved vertical and horizontal resolutions and instrument observation accuracy. With current planning, the next-generation Advanced Technology Microwave Sounder to be flown on National Polar-orbiting Operational Environmental Satellite System Preparatory Project and Joint Polar Satellite System will replace the Advanced Microwave Sounding Unit (AMSU) to carry the satellite microwave sounding capability into the future.

[5] The MSU/AMSU observations have been playing a vital role in accurate NWP. The direct use of the MSU radiance data in NWPs was demonstrated to considerably improve NWP forecast skills in earlier data assimilation experiments [*Derber and Wu*, 1998]. With improved resolution and instrument accuracy, the AMSU observations had led to further improvement in NWP forecast skills [e.g., *English et al.*, 2000]. Those improvements are mostly attributed to the near-all weather observation capabilities in MSU/AMSU. At present, the AMSU data are used in most NWP forecast centers in the world to provide key information for improved NWP forecast accuracies.

[6] Because of its long-term continuity, global coverage, and insensitivity to cloud effects, the MSU/AMSU measurements have also been the primary source for determining the global atmospheric temperature trends and variability. Different versions of the MSU/AMSU upper-air temperature CDRs have been generated by different research groups for atmospheric temperature trend detections, including the University of Alabama at Huntsville group [*Spencer and Christy*, 1992; *Christy et al.*, 2003], the Remote Sensing Systems (RSS) group [*Mears et al.*, 2003; *Mears and Wentz*, 2009], and the NOAA/Center for Satellite Applications and Research (STAR) group [*Zou et al.*, 2006, 2009; *Zou and Wang*, 2010]. The MSU/AMSU observations are also one of the most important input data sets in climate modeling reanalysis developments [e.g., *Dee and Uppala*, 2009; *Saha et al.*, 2010; *Rienecker et al.*, 2011], which in turn were the most widely used data sets for climate research.

[7] The MSU atmospheric sounding channels onboard TIROS-N through NOAA 14 had been intercalibrated using their SNOs in the study by *Zou et al.* [2006, 2009]. The intercalibration significantly reduced scene temperature dependent biases and time-varying intersatellite biases related to sun-heating-induced instrument temperature variability, resulting in a consistent set of radiance fundamental climate data record (FCDR). The 20 year SNO intercalibrated MSU data covering the years 1987–2006 were assimilated by the new generation of NOAA/National Centers for Environmental Prediction Climate Forecast System Reanalysis and NASA's Modern Era Retrospective-analysis for Research and Applications (MERRA) reanalysis. Improved satellite bias correction patterns have been seen in these reanalyses with the intercalibrated MSU data [*Saha et al.*, 2010; *Rienecker et al.*, 2011]. This radiance FCDR was also used to generate the STAR version of the long-term MSU/AMSU atmospheric temperature thematic climate data record (TCDR). One advantage in using the FCDR for TCDR development is that the instrument calibration errors were corrected early on in a homogeneous way. In this fashion, these errors were prevented from propagating to the gridded temperature analysis level where, if not corrected, they could couple with the diurnal drift errors, causing uncertainties in bias corrections and uncertainties in trend calculations [*Zou et al.*, 2009; *Zou and Wang*, 2010].

[8] This study focuses on intersatellite calibration of the AMSU-A sounding channels onboard NOAA 15, 16, 17, and 18, on MetOp-A, and on Aqua. Using overlap observations, we identify and analyze five different types of calibration errors existing in the prelaunch-calibrated AMSU-A observations, which include relatively stable intersatellite biases between most satellite pairs, bias drifts on NOAA 16 and certain channels on MetOp-A, sun-heating-induced instrument temperature variability in satellite radiances, scene temperature dependency in biases due to inaccurate calibration nonlinearity, and biases due to channel frequency shift from its prelaunch measurement in NOAA 15 channel 6. The first, third, and fourth types of biases were also found in MSU observations [*Zou et al.*, 2006]; therefore, the intercalibration algorithm developed for the MSU instrument is applied to remove or minimize these errors. In addition, time-dependent coefficients are introduced in the calibration algorithm to minimize bias drifts, which are special features in AMSU-A observations on NOAA 16 and MetOp-A.

[9] Of particular note, the radiative transfer models in the NWP and reanalysis data assimilation systems generally adopt channel frequency values from prelaunch measurements to simulate the satellite observations, based on the belief that those frequency values were the same before and after satellite launch. However, the SNO analysis in this study provides evidence that certain satellite channels, such as NOAA 15 channel 6, incurred a central frequency shift after satellite launch. This type of error was not found in previous MSU studies. We use radiative transfer model

simulations at satellite SNO sites to find the actual post-launch channel frequency values. The corrected channel frequency is expected to improve AMSU-A applications in both NWP and climate reanalysis data assimilations where accurate channel frequency values are required. Although only one channel is corrected for the frequency shift in this study, the analysis method is expected to be applicable to other channels or instrument observations exhibiting similar biases.

[10] The level-1c AMSU-A intercalibration and our previous MSU intercalibration are independent of each other. However, their resulting FCDRs are merged together to generate STAR version 2.0 of MSU/AMSU upper-air temperature TCDR, including temperatures of midtroposphere, upper troposphere, and lower stratosphere. The AMSU-only temperature time series are also generated for channels without the MSU equivalents. The procedure for generating these data sets is summarized in this study.

[11] The article is structured as follows: Section 2 describes the AMSU-A level-1c data calculated from satellite measurements (so-called calibration procedure). Section 3 analyzes satellite overlap observations to identify and classify calibration errors in the AMSU-A prelaunch calibration. Section 4 explains how the SNO intercalibration approach is used to estimate improved calibration coefficients for use by the calibration procedure in removing or minimizing nonlinear calibration errors. Section 5 describes an SNO analysis method to determine channel frequency shift. Section 6 describes the merging procedure for STAR version 2.0 MSU/AMSU atmospheric temperature data set. Section 7 provides a summary and conclusion.

2. Level-1c Calibration Equation for AMSU-A

[12] The generation of level-1c radiances from raw AMSU-A observations that are stored in level-1b files requires application of a so-called calibration equation. The equation described by *Zou et al.* [2006, 2009] for the MSU instrument applies also to the AMSU-A instrument. Similar to MSU, the AMSU-A calibration relies on two calibration targets as end point references: a cosmic space "cold" target and an onboard blackbody "warm" target. The cold space has a temperature of 2.73 K, and the warm target temperature is measured by platinum resistance thermometers (PRTs) embedded in the blackbody target. In each scan cycle, the instrument looks at these two targets, as well as Earth, and the signals in the form of electric voltage are processed by the instrument and finally converted to digital counts through an analog-to-digital converter. These digital counts are output as raw observations in AMSU level-1b files.

[13] The AMSU-A level-1c calibration equation transfers the raw counts to the radiances using the two calibration targets as follows [*Zou et al.*, 2006, 2009]:

$$R = R_L - \delta R + \mu Z, \tag{1}$$

where R is the Earth scene radiance, $R_L = R_c + S(C_e - C_c)$, representing the dominant linear response, and $Z = S^2(C_e - C_c)(C_e - C_w)$ is a nonlinear response characterizing the nonperfect square law nature of a detector or a nonlinear amplifier. C represents the raw counts value of the satellite observations and $S = (R_w - R_c)/(C_w - C_c)$ is the slope determined by the two calibration targets. The subscripts e, w, and c refer to the Earth view, onboard blackbody warm target view, and cold space view, respectively; δR represents a radiance offset; and μ is a nonlinear coefficient representing the magnitude of the calibration nonlinearity. The cold space reference temperature is assumed to be 4.78 K, which includes the actual cold-space temperature of 2.73 K plus an increase of about 2 K due to the antenna sidelobe radiation. This is the same as that assumed for the MSU sidelobe effect [*Zou et al.*, 2006] but different from the AMSU-A prelaunch calibration where channel-dependent sidelobe correction was applied to the cold-space temperature. The impact of these different specifications of sidelobe effect will be further discussed later in the calibration section. The algorithms described in the NOAA KLM User's Guide [*Robel*, 2009] are used to compute R_w for each AMSU-A channel. Once the offsets and the nonlinear coefficients are known, radiance is computed through equation (1), and the brightness temperature, T_b, is then computed using the Planck function.

[14] Equation (1) is a modified version of the algorithm used by NOAA for operational generation of the level-1c products, where δR was assumed to be 0 and the nonlinear coefficient μ was determined from prelaunch laboratory tests [*Mo*, 1996]. These coefficients have been converted to polynomial coefficients with respect to scene counts [*Robel*, 2009] and then stored in AMSU-1b files. Radiances calculated using coefficients in AMSU-1b files are hence referred to later as the operational calibration. However, because this procedure was repeated for each AMSU-A instrument independently, it was not designed to correct for residual biases between satellites.

[15] In the intersatellite calibration described in this study, the offset δR in equation (1) allows for the removal of intersatellite differences. In addition, the calibration coefficients, δR and μ, were determined using SNO matchups. There are other differences with the operational calibration. For example, the raw counts values of the calibration targets in equation (1) were averages over seven adjacent scan lines in the operational calibration [*Mo*, 1996]. However, in our intersatellite calibration, target counts values of a single scan line were used to calibrate each Earth scene observation in that scan line. This change was made because SNOs are collected for individual near-nadir footprints. When deriving calibration coefficients from SNOs, target observations closest to the SNO footprints, which are those from the same scan lines of the SNO events, are used to eliminate potential nonsimultaneous errors. Limited experiments indicate that this change may increase the noise in the level-1c radiances by 2% compared to those using the original method of averaging adjacent scan lines. This small extra noise is not expected to affect the quality of the resulting level-1c radiances. However, if future evidence suggests that this will cause large errors in the weather and climate reanalysis data assimilations, we will use the operational algorithm for target counts calculation but with the SNO calibration coefficients applied.

[16] Quality control procedure in the operational calibration is used in the SNO intercalibration to deal with the missing calibration information, instrument anomalies, and bad scan lines. Unless otherwise specified, the processing details described later in this study apply to the intersatellite calibration.

Table 1. Channel and Scanning View Numbers for the MSU and AMSU-A Antenna Systems

Instrument Antenna Systems	MSU-1	MSU-2	AMSU-A A1–1	AMSU-A A1–2	AMSU-A A2
Channels	1–2	3–4	6–7, 9–15	3–5, 8	1–2
Earth views per scan line	11	11	30	30	30
Blackbody and space views per scan line	1	1	2	2	2
PRTs in each warm target	2	2	5	5	7

[17] Each scan line in the AMSU-A observations contains 30 Earth views, 2 space views, and 2 warm target views. The PRTs on each target ranges from 5 to 7, depending on specific channels. The average of the 2 space views and blackbody views are used to calibrate the 30 Earth views. The warm target temperature, T_w, is the average of the available good PRT measurements for each instrument. In general, there is a warm target for each antenna system, but there are more than one antenna systems for each instrument unit. These units and antenna systems for AMSU-A are listed in Table 1, along with the MSU instrument units for comparison. This study extensively discusses channels 5 (53.596 $\pm$ 0.115 GHz, double bands), 6 (54.4 GHz, single band), 7 (54.94 GHz, single band), and 9 (57.29 GHz, single band), where channel 5 uses A1–2 antenna system, and the other 3 channels use A1–1 antenna system. AMSU-A channels 5, 7, and 9 are the equivalent channels for MSU channels 2, 3, and 4, although channel frequencies are slightly different between the 2 instruments for each companion channel. Although not extensively discussed, we also provide calibration coefficients for other channels and their comparisons to operational calibration.

3. Issues in AMSU-A Operational Calibration

[18] Prior to presenting the results of the intersatellite calibration of AMSU-A observations, we first analyze the calibration errors that need to be dealt with. We use SNOs and global ocean mean differences to characterize the instrument calibration errors. The SNO concept was drawn from the fact that the nadir ground tracks from two polar-orbiting satellites are circles; these circles typically intersect at two points in the vicinity of the North and South Poles [*Cao et al.*, 2004]. For NOAA morning and afternoon polar-orbiter pairs, every 7–10 days, the actual satellites pass over these intersection points within 30–60 s of each other. The SNO matchups for the AMSU-A instrument onboard satellites NOAA 15 through NOAA 18 and MetOp-A were accumulated using the algorithm in the study by *Cao et al.* [2004]. The distance and time criteria for the SNO matchups were set to be 45 km and 50 s, respectively. These matchups are free from sampling errors such as the diurnal drift errors; therefore, their statistical differences represent instrument calibration errors in the satellite pairs.

[19] However, noise due to small time differences and nonzero nadir distances in the SNOs causes difficulties for them to characterize certain fine features such as the instrument temperature effect on the calibration. On the other hand, a global intersatellite bias analysis indicated that diurnal drift errors can be ignored over the oceans for the MSU channel 2 and globally for the MSU channels 3 and 4 [*Zou et al.*, 2009; *Zou and Wang*, 2010]. Similarly, diurnal effect is found negligible over oceans for channels 4 and 5 and globally for channels 6–10 of AMSU-A observations. As diurnal effects can only be seen from the intersatellite bias analysis when calibration errors have been removed, justification on the above statement will be presented in section 4 after the intercalibration procedure is completed. At this point, it is taken as a known fact that diurnal effect is negligible over oceans for AMSU-A channels 4–10. For these channels, noise is canceled out in the averaging processes, thus the global ocean mean analyses are fairly efficient in characterizing instrument temperature-related calibration errors. For channels 11–14, the diurnal effect is large because of strong solar semidiurnal tides in the stratosphere. However, our experiments with and without diurnal drift corrections for these channels suggest that diurnal effect does not affect the level-1c calibration. This occurs because the diurnal effect is uncorrelated to the instrument temperature variability, allowing the two processes to be treated separately. Therefore, throughout this study, we use the SNOs and global ocean means to complement each other in characterizing and even in developing methodologies to remove or minimize calibration errors.

[20] Figure 1 shows local equator crossing time for NOAA 15, 16, 17, and 18 and MetOp-A, from which one can see orbital drifts and overlapping periods between satellite pairs. Table 2 lists the launch time, data analysis period, and the current status for these satellites. As there are no data for NOAA 15 channels 11 and 14 since pre-2000s, these two channels are not intercalibrated in this study. Figure 2 shows intersatellite difference time series for the operational calibrated, global ocean mean T_b for AMSU-A channels 5, 6, 7, and 9 for these satellites. The global ocean mean is defined as the average of 22 near-nadir, limb-corrected AMSU-A T_b in each scan line over the global ocean for each satellite. Examinations of these difference time series reveal several issues in the operational calibration of AMSU-A.

[21] 1. Constant intersatellite biases: Relatively stable or constant intersatellite biases exist for most satellite pairs (e.g., channels 7 and 9, for the pairs of NOAA 15 and NOAA 18 and NOAA 15 and Aqua). As mentioned earlier, this is because prelaunch laboratory calibration was conducted independently, and the calibration offsets could vary by satellite. Antenna pattern and satellite altitude differences could be other factors causing these biases. These biases can be removed by adjusting calibration offsets.

[22] 2. Bias drifts: There are obvious steady bias drifts in all satellite pairs involving NOAA 16 for channels 5, 7, 9, and other channels (not shown) before 2008. Similar drifts also occur for MetOp-A channel 7. The rates of the drifts between NOAA 16 and NOAA 15 are about 0.2–0.5 K per decade, which are significant enough to cause climate trend debate when different satellite observations are used for climate trend detection. Note that intersatellite T_b differences for satellite pairs between Aqua and NOAA 15 and between NOAA 18 and NOAA 15 are quite stable during their relatively long overlapping observation periods, except for

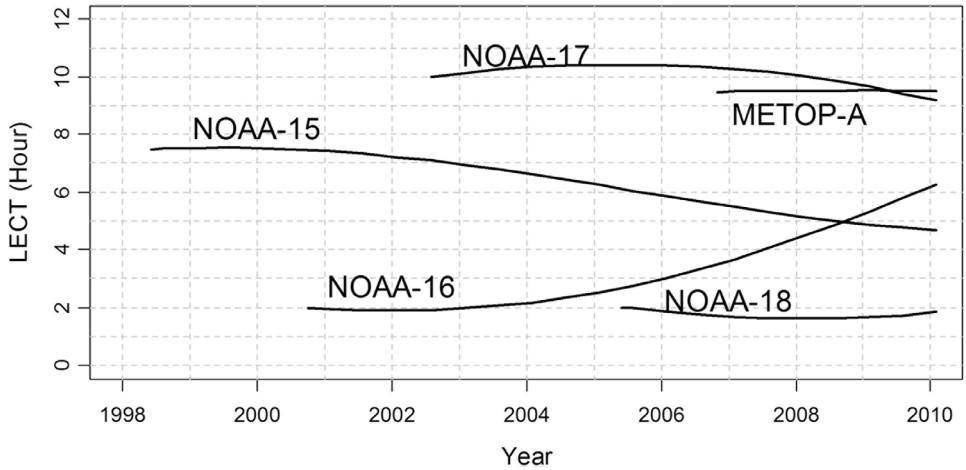

Figure 1. Local equator crossing time of descending orbits of the operational NOAA and MetOp-A satellites.

channel 6. These suggest that NOAA 16 may have a bias drift that needs to be corrected. *Mears and Wentz* [2009] also noticed the NOAA 16 bias drift and did not use this satellite in their MSU/AMSU time series generation. To gain a better understanding of this drift, we examine the global ocean mean raw counts data of NOAA 16 and NOAA 15 in Figure 3. When viewed in terms of global ocean means, one may postulate that the natural weather variability in the Earth view counts largely cancel out between the Southern and Northern Hemispheres (except for years when there are large interannual variability related to El Niño–Southern Oscillation and Arctic Oscillation, etc.), so that over time only the instrument-related variability were revealed. It is seen that the NOAA 15 raw counts exhibit a fair long-term (decadal) stability for all the Earth scene, cold target, and warm target views except for a sun-heating-induced seasonal and interannual variability (see Figure 4 and associated discussions). However, the raw counts for NOAA 16 exhibit decreasing long-term drifts for all its Earth and target views, including the cold-space views, which is more puzzling. The reason for these drifts remains unknown, and in any case, the operational calibration failed to account for these drifts. In this study, time-dependent calibration offsets are introduced later on to minimize these drifts.

[23] 3. Sun-heating-induced instrument temperature variability in T_b: For channel 6 (Figure 2b), intersatellite T_b differences for satellite pairs involving NOAA 15 contain a seasonal and interannual variability. Similar variability was found for satellite pairs involving NOAA 16 after 2008 for most channels (Figures 2a–2d) and for MSU observations [*Christy et al.*, 2000; *Zou et al.*, 2006]. Our study indicated that this is related to the sun-heating differences on the instrument, which can be characterized by Solar Beta Angle (SBA) defined as the solar angle relative to the satellite normal. Figures 4a and 4b show the NOAA 15 and NOAA 16 warm target temperature time series, respectively, along with their SBA time series. It is seen that the SBAs of both satellites exhibit seasonal variability with yearly differences due to satellite orbital drifts. For NOAA 15, changes in its SBA cause sun-heating variations on the instrument, which further results in instrument temperature changes. As seen, the warm target temperature, which is at the instrument ambient temperature and thus referred to as the instrument temperature below, follows closely the SBA variations, except when the SBAs are low (50°–55°). The high correlation coefficient between the two time series, at 0.85, confirms this finding. Note the large warm target temperature variability over the time period shown, with amplitude of about 20 K.

[24] Similar instrument variability was found for NOAA 16 after 2008 when its orbit drifted close to NOAA 15 (Figure 2). Before 2008, however, the SBA of NOAA 16 gradually increased from 20° to 60°, but its instrument temperature remained relatively stable with its variability not well correlated to changes in SBA. This occurred most likely because, for low SBAs before 2008, the satellite solar shield was orientated in a direction that it could effectively protect the instrument from solar illumination. After 2008, however, certain amount of solar radiation passed through or bypassed

Table 2. Satellite Launch Time, Data Analysis Period, and Current Status for the Satellites of Interest

Satellite	Launch Time	Data Start Time	Data End Time	Current Status
NOAA 15	13 May 1998	26 Oct 1998	31 Dec 2010	Still operating; channel 11 failed on 10 Apr 2002; channel 14 no data since 30 Oct 2000
NOAA 16	21 Sep 2000	1 Jan 2001	31 Dec 2010	Still operating; channel 4 no data since 4 Mar 2008
NOAA 17	24 Jun 2002	28 Jun 2002	30 Sep 2003	AMSU-A1 powered off on 30 Oct 2003
NOAA 18	20 May 2005	24 May 2005	31 Dec 2010	Still operating
MetOp-A	19 Oct 2006	1 Jan 2007	31 Dec 2010	Still operating
Aqua	4 May 2002	23 May 2002	31 Dec 2010	Still operating

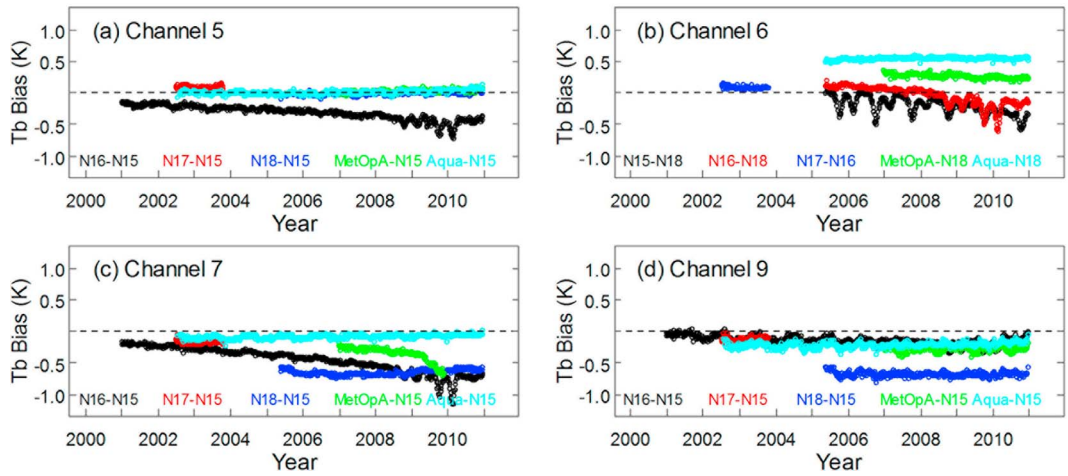

Figure 2. Global ocean mean intersatellite T_b difference time series for AMSU-A operational calibration for satellites NOAA 15, 16, 17, and 18; MetOp-A; and Aqua for different channels. Differences are chosen against the reference satellites; thus, the satellite pairs shown for channel 6 are different from other channels (see section 4).

the solar shield after its orientation was changed because of orbital drift, causing instrument temperature to vary with SBA.

[25] The changes in instrument temperature further cause variations in the spacecraft thermal emission, which are received as part of the signals in the antenna sidelobe views of Earth and calibration targets (Figure 3). For channels having a linear relationship between the instrument outputs (raw counts) and radiances of a target being measured, the spacecraft thermal emission signals can be mostly removed by the linear calibration equation. In fact, operational calibration equations are nearly linear for most channels because nonlinear calibration coefficients determined from prelaunch laboratory tests are generally small (see *Mo* [1996] and discussions in section 4 below). The fact that the instrument temperature variability does not show up in the intersatellite difference time series between NOAA 15 and most other satellites in channels 5, 7, and 9 (Figure 2) suggests that prelaunch calibration works well for these channels. In other words, NOAA 15 channels 5, 7, and 9 are nearly linear channels. However, because of the existence of the instrument temperature variability in the T_b time series, NOAA 15 channel 6 and most NOAA 16 channels are believed to have a high calibration nonlinearity that was not accurately represented by the operational calibration. As had been demonstrated in the study by *Zou et al.* [2006, 2009], inaccurate expressions of the nonlinearity cause residual instrument temperature variability to manifest in its radiance time series. To quantify this phenomenon, the correlation coefficient between the time series of NOAA 15 T_w and the time series of T_b differences between NOAA 16 and NOAA 15 channel 6 is as large as 0.85. Note that before 2008, NOAA 16 radiances did not feature instrument temperature variability for most channels. This is not because these channels are nearly linear, but because variability of the instrument temperature was small.

[26] In addition to the sun-heating-induced instrument temperature variability, NOAA 15 channel 6 also exhibits bias drift (Figure 2b). Furthermore, as seen later on, its channel frequency has a shift from its prelaunch measurement. The fact that NOAA 15 channel 6 features all these different types of errors makes its calibration more challenging.

[27] 4. Scene temperature dependent biases due to inaccurate calibration nonlinearity: In addition to instrument temperature effect, inaccurate nonlinearity in the calibration equation also causes intersatellite biases to depend on the scene temperature [*Zou et al.*, 2006], which further causes biases to depend on latitudes and seasons. *Zou et al.* [2009] examined in detail the latitudinal dependency in residual

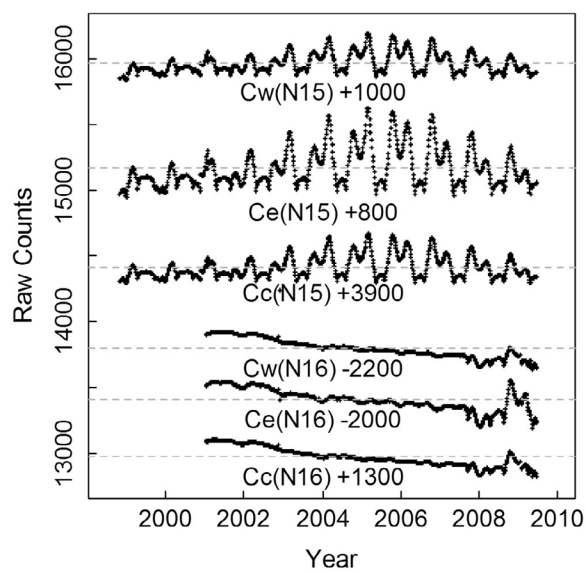

Figure 3. Global ocean mean time series of the raw counts data for Earth, warm target, and cold-space views for channel 5 on NOAA 15 and NOAA 16, respectively. The original count values have been rescaled, so that all different curves are plotted in a single panel. The counts symbols in the plot are consistent with equation (1).

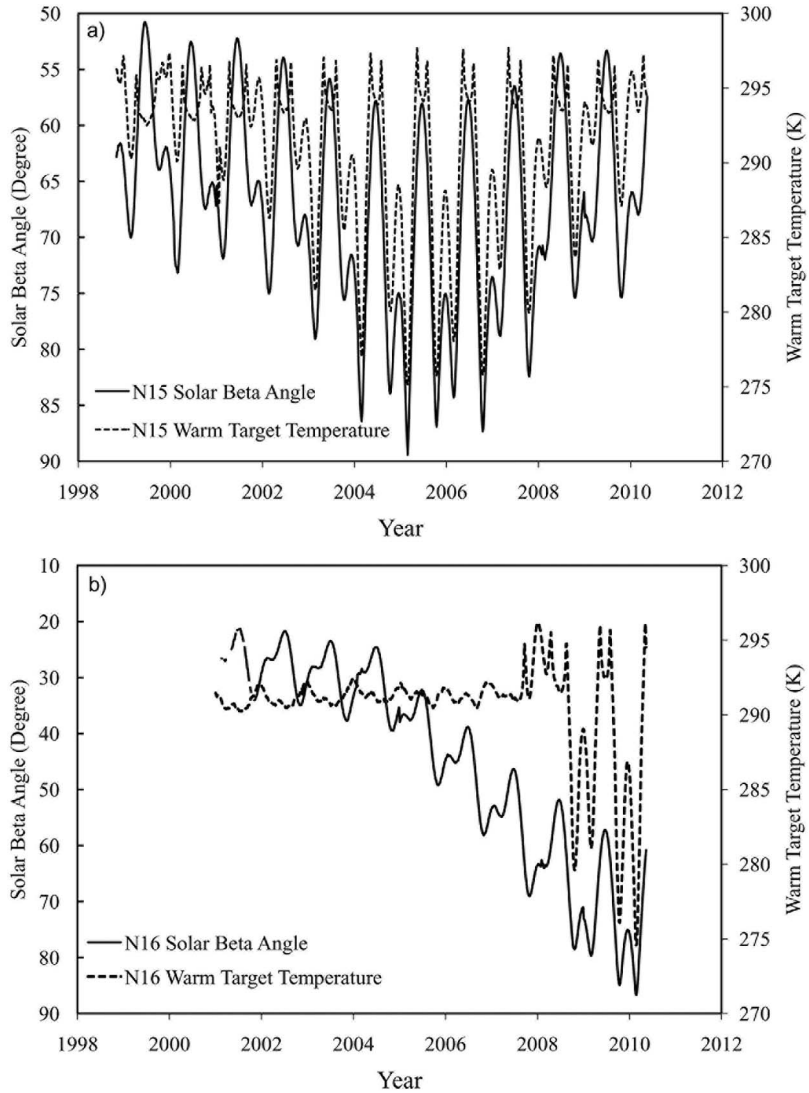

Figure 4. Warm target temperature and Solar Beta Angle time series for (a) NOAA 15 and (b) NOAA 16. The correlation coefficients between the two time series are 0.84 for NOAA 15 and 0.49 for NOAA 16, respectively.

intersatellite biases for the MSU observations after the SNO calibration between most satellite pairs. In Figure 5, as an example, we show a seasonal dependency in the SNO T_b time series between MetOp-A and NOAA 18 due to the scene temperature dependency in biases. The reasoning chain for understanding these plots is as follows. First, unrealistic nonlinear calibration coefficients were assigned to the calibration equation (1) for both MetOp-A and NOAA 18 channel 6 observations. This results in obvious scene temperature dependent biases as shown by the bias slope in Figure 5a. As a result, MetOp-A T_b is about 1 K lower than the NOAA 18 T_b for lower temperatures, while they are about the same for higher temperatures. Second, the scene temperature dependent biases cause seasonal cycles in the SNO time series between the two satellites with opposite phases over the Arctic and Antarctic as shown in Figures 5b and 5c. As seen, during winter (summer), when temperature is lower (higher), the MetOp-A T_b is about 1 K lower than (about the same as) the NOAA 18 T_b over both Arctic and Antarctic (note that the Arctic winter is the Antarctic summer and vice versa). This seasonal variation corresponds well with Figure 5a, indicating a close causal relationship between scene temperature dependency and seasonal dependency in biases. Also, note that this out-of-phase seasonality in the Arctic and Antarctic SNO time series cannot be explained by the instrument temperature variability of either MetOp-A or NOAA 18.

[28] 5. Biases due to channel frequency errors: Channel frequency values were generally assumed to be equal to the prelaunch specifications or measurements in NWP and climate reanalysis data assimilations as well as other applications of the MSU/AMSU observations. However, the actual frequency values could be different from the prelaunch specifications or measurements due to postlaunch instrument errors. Radiance biases caused by the frequency errors may mix with the nonlinear calibration errors; thus, it is

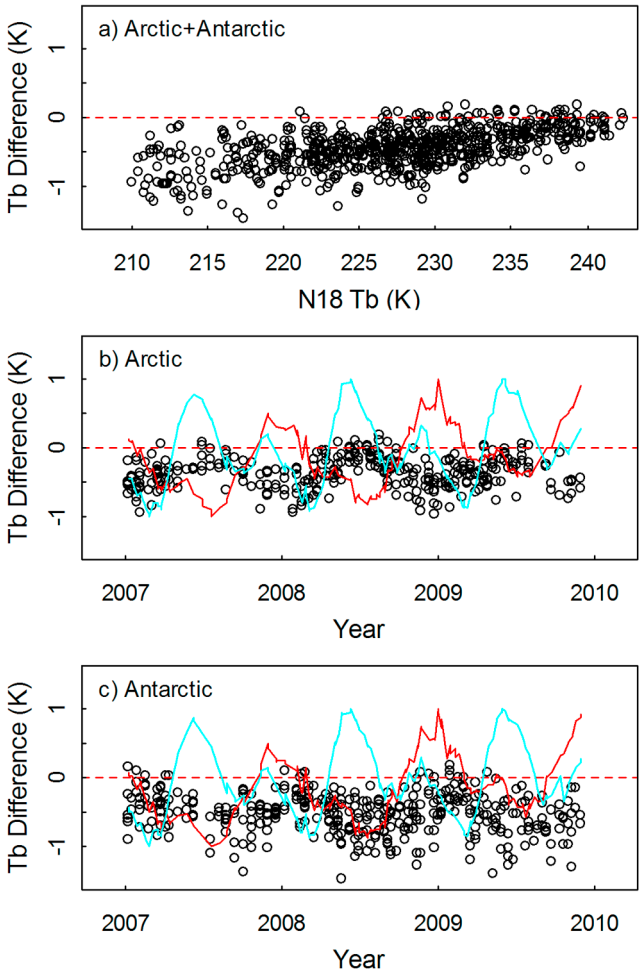

Figure 5. SNO plots showing how scene temperature dependent biases cause seasonal cycles with opposite phases in the Arctic and Antarctic SNO time series. (a) SNO scatterplot for T_b (N18) versus $\Delta T_b = T_b$ (MetOp-A) $- T_b$ (N18), (b) SNO time series for T_b (MetOp-A) $- T_b$ (N18) over the Arctic, and (c) same as Figure 5b except over the Antarctic. The red and blue curves in Figures 5b and 5c are the warm target temperature time series for MetOp-A and NOAA 18, respectively.

sometimes difficult to differentiate errors between the two sources. In this study, we develop an SNO methodology to identify this error. The SNO bias characteristics caused by channel frequency differences were analyzed in the study by *Iacovazzi et al.* [2009] using MSU and AMSU-A equivalent channels. Essentially, channel frequency differences result in two satellites viewing different layers of the atmosphere, and thus, the observed T_b are different when there is a nonzero lapse rate in the atmosphere. These differences translate to seasonal cycles in the SNO time series that have phases and amplitudes tied closely to the lapse rate climatology over the Arctic and Antarctic regions. As an example, Figure 6 shows the Arctic and Antarctic SNO time series for AMSU-A channel 6 observations between NOAA 15 and NOAA 18. The seasonal cycles with opposite phases in Figures 6b and 6c are at first sight similar to Figures 5b and 5c where scene temperature dependent biases were inferred from inaccurate nonlinear calibration. In Figure 6, however, the nonlinear calibration coefficients are sufficiently accurate in removing nonlinearity-related scene temperature dependency in biases, as seen later on in the calibration section. In addition, the remaining scene temperature dependency in biases (Figure 6a) has the shape of "S" lying on its side that is very different from that in Figure 5a. This type of scene temperature dependent biases and their associated seasonality in the SNO time series are believed to be caused by a frequency shift in NOAA 15 channel 6. Further discussion on this is presented later in section 5 when we intend to

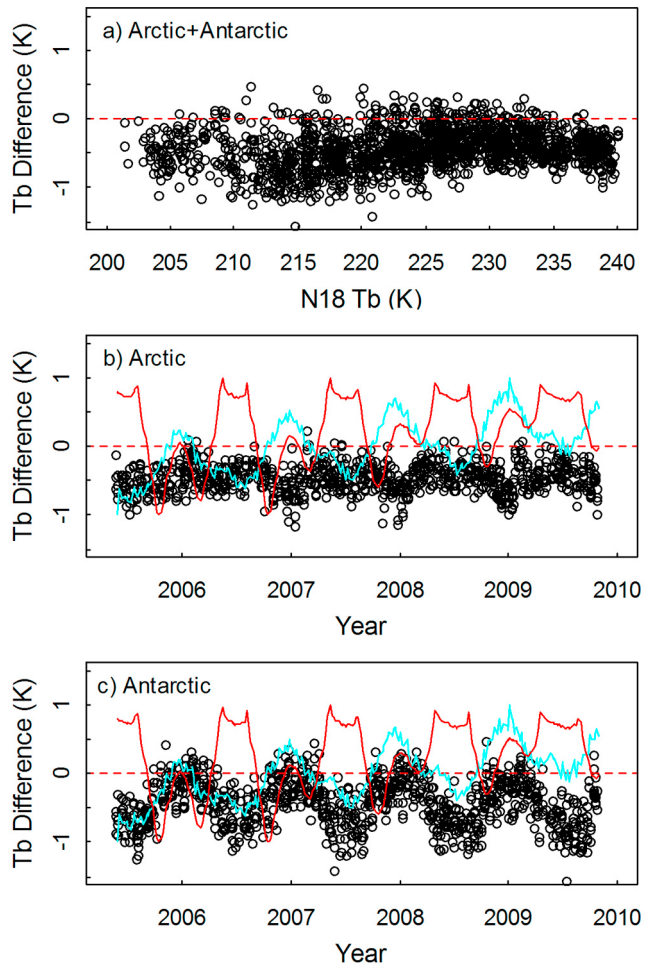

Figure 6. (a) SNO scatterplot for T_b (N18) versus $\Delta T_b = T_b$ (N15) $- T_b$ (N18), (b) SNO time series over the Arctic for $\Delta T_b = T_b$ (N15) $- T_b$ (N18), and (c) same as Figure 6b except over the Antarctic. The T_b data in these plots were derived using the calibration coefficients in Table 3 where calibration nonlinearity-related scene temperature dependent biases have already been minimized in the following SNO calibration procedure. In addition, NOAA 15 offset has been adjusted to account for its frequency shift as found in section 5, so its T_b values are lower than operational calibrated values by a constant. The red and blue curves in Figure 6b and 6c represent the warm target temperatures of NOAA 15 and NOAA 18, respectively.

determine the actual frequency shift using radiative transfer model simulations.

4. Determining Instrument Calibration Nonlinearity and Intersatellite Offsets Using the SNO

[29] *Zou et al.* [2006, 2009] developed an intercalibration method relying on sequential SNO and applied it to the MSU instrument onboard different satellites. The method significantly reduced MSU calibration errors, including the sun-heating-induced instrument temperature variability in radiances, intersatellite biases, and their scene temperature dependency. The same method is applied to intercalibrate AMSU-A for satellites NOAA 15, 16, 17, and 18 and MetOp-A. Because of the unfortunate unavailability of AMSU-A instrument raw counts for Aqua, the full SNO method could not be applied to that satellite. Instead, we could only compute constant offsets for Aqua (see in the following).

[30] In the sequential regression method, a reference satellite needs to be selected, so that its calibration offset, δR, and nonlinear coefficient, μ, are assumed to be known temporarily. Subsequent calibration offsets and nonlinear coefficients of all other satellites are determined sequentially (one by one) from regressions of the SNO matchups between satellite pairs, starting from the satellite closest to the reference satellite. The calibration offset, δR, was arbitrarily set to be 0 for the reference satellite, because it does not affect the climate variability and trends. However, we note that for applications that would consider these observations as absolute references (e.g., for data assimilation), this particular point would need to be taken care of. We discuss this point later in section 7.

[31] For AMSU-A observations, the reference satellites are selected to be NOAA 18 for channel 6 and NOAA 15 for all other channels. For the sequential procedure to complete, a satellite should at least overlap with another satellite for a time period long enough to resolve the sun-heating-induced instrument temperature variability. A minimum requirement for the overlap to cover a complete cycle of the instrument temperature variability and to avoid calibration uncertainties due to short overlap problems is 1 year. These requirements are basically satisfied by the AMSU-A satellites to be intercalibrated (Figures 1 and 2 and Table 2), although there are only 15 months of data for NOAA 17, which may potentially cause it to have larger calibration uncertainties than others. In any case, with the overlapping condition satisfied, the sequential procedure actually reduces the problem to the determination of the nonlinear coefficient, μ, of the reference satellite; once it is known, calibration nonlinear coefficients for all other satellites are solved from the SNOs.

[32] The nonlinear coefficient, μ, of the reference satellite was determined under the constraint that the averaged sun-heating-induced instrument temperature variability in the radiances for all satellite pairs should be minimal. To meet this requirement, a series of sensitivity experiments was conducted in which the nonlinear coefficient of the reference satellite was selected at different values within a reasonable range. For each given value, a set of calibration offsets and nonlinear coefficients for all other satellites was obtained sequentially from regressions of the SNO matchups. For each set of calibration coefficients, level-1c radiances were generated for all satellites, and the sun-heating-induced instrument temperature variability were examined in the global ocean mean, T_b, difference time series. The final determination of the nonlinear coefficient of the reference satellite was made when the average of this variability is minimal for all satellites. This approach generates a set of level-1c radiances that does not depend on the initial selection of the reference satellite.

[33] The above procedure can be summarized as follows:

[34] 1. First choose a value for μ_{N15} and set $\delta R_{N15} = 0$ (or choose a value for μ_{N18} and set $\delta R_{N18} = 0$ when NOAA 18 is chosen as the reference satellite).

[35] 2. Use SNO regressions to obtain $\mu_{N15} - \mu_k$ and $\delta R_{N15} - \delta R_k$, for $k = 1, 4$, where k refers to satellites NOAA 16, 17, and 18 and MetOp-A (note that NOAA 15 has overlaps with all other satellites).

[36] 3. Generate level-1c radiances for all satellites including the reference satellite using μ_k and δR_k for $k = 1, 5$.

[37] 4. Compute global ocean mean time series of $T_{b,j} - T_{b,k}$ for available overlaps between satellites j and k, where j and k are satellite indexes.

[38] 5. Change the value of μ_{N15} and repeat steps 2, 3, and 4.

[39] 6. Stop when summation of root mean square of $(T_{b,j} - T_{b,k})$ is minimum.

[40] By design, the sequential method searches for three optimum parameters to minimize three types of calibration errors in satellite pairs. (1) Optimum value of the offset differences between satellites j and k, $\Delta\delta R = \delta R_j - \delta R_k$, minimizes constant intersatellite biases. (2) Optimum difference between the nonlinear calibration coefficients of the two satellites, $\Delta\mu = \mu_j - \mu_k$, minimizes scene temperature dependency in biases. (3) Optimum absolute values of either μ_j or μ_k minimize the sun-heating-induced instrument temperature variability in the radiances. Using NOAA 15 and NOAA 16 satellite pairs as an example, Figure 7 visually demonstrates how optimum calibration coefficients were obtained from the SNO calibration procedure. In the plot, the quadratic curves in each panel, respectively, represent calibration equations for NOAA 15 and NOAA 16 for a specific combination of the nonlinear coefficients, μ_{N15} and μ_{N16}, with their differences, $\mu_{N15} - \mu_{N16}$, determined by their SNO matchups. Also shown in each panel is their SNO T_b difference time series corresponding to the calibration curves within the panel. Changing the calibration coefficient, μ_{N15}, of the reference satellite also changes μ_{N16} because of their SNO constraint. These changes resulted in graduate changes in magnitude from Figures 7a–7d of the sun-heating-induced instrument temperature variability in their SNO T_b difference time series. Only a unique combination of the calibration coefficients μ_{N15} and μ_{N16} minimizes the instrument temperature variability (Figure 7c). For a detailed description of the procedure, the readers are referred to *Zou et al.* [2006, 2009] and *Zou and Wang* [2010].

[41] In the MSU case, the optimum constant calibration coefficients were obtained from the above procedure for all satellites [*Zou et al.*, 2009]. For the AMSU-A observations, however, time-dependent offsets and nonlinear coefficients are further introduced for certain channels to account for their bias drifts as found in Figure 2. To be specific, we assume that the calibration offset varies as follows for

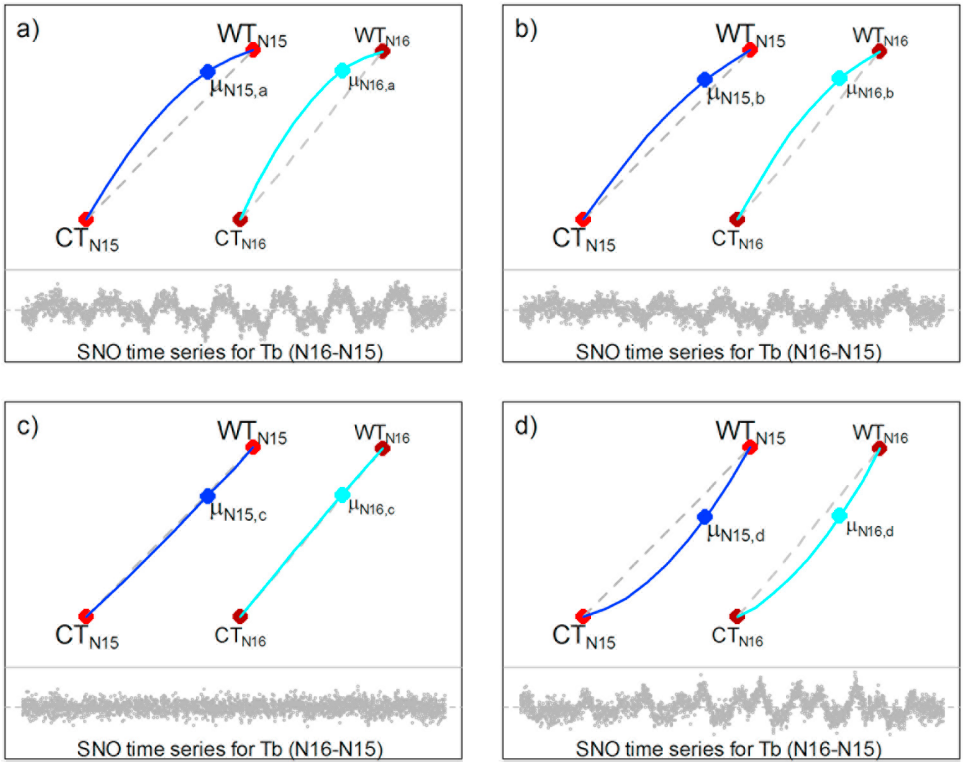

Figure 7. Schematic plots showing how sun-heating-induced instrument temperature signals in radiances were removed by an appropriate combination of the nonlinear calibration coefficients between two satellites. In each panel, the top two quadratic curves represent calibration equations for NOAA 15 and NOAA 16, respectively, corresponding to different values of nonlinear coefficients μ_{N15} and $\mu_{N16,}$ where the horizontal coordinate represents the raw counts and the vertical coordinate represents the radiance. Symbols CT and WT stand for cold and warm targets, respectively. The lower time series are SNO T_b differences for channel 7 between the two satellites (NOAA 16 minus NOAA 15) with horizontal coordinates being the time and vertical coordinates being the T_b differences. In the plot, the changing δR_{N16} effect was taken out of the data first, so the NOAA 15 and NOAA 16 difference time series appear to be flat for Figure 7c.

NOAA 15 channel 6, MetOp-A channel 7, and most NOAA 16 channels:

$$\delta R = \delta R_0 + \kappa(t - t_0), \tag{2}$$

where δR_0 is a constant offset, κ is a rate of changes in the offset, t is the time, and t_0 is a reference time that can be the satellite launch time or any other reference time when the offset begins to change. As demonstrated later, this simple calibration offset model is sufficient to remove the bias drifts in NOAA 16 and MetOp-A channel 7. However, it is insufficient to remove the bias drift in NOAA 15 channel 6. For this channel, we construct a simple model for the nonlinear coefficient:

$$\mu = \mu_0 + \lambda(t - t_1), \tag{3}$$

where μ_0 is a constant nonlinear coefficient, λ is the rate of changes of the nonlinear coefficient, and t_1 is another reference time.

[42] When solving for the calibration coefficients in equations (2) and (3), δR_0 and μ_0 were obtained first from the SNO sequential procedure described earlier with κ and λ being assumed to be 0. The resulting δR_0 and μ_0 were then fixed in subsequent procedures in determining κ and λ values. To obtain κ and λ, a series of sensitivity experiments were conducted in which κ and λ were selected within a reasonable range, and different sets of level-1c radiances were computed corresponding to these different values. The final selection of κ and λ was made when the intersatellite bias drifts of the global ocean means are minimal for the respective intercalibrated channels.

[43] The resulting calibration coefficients for channels 4–10, 12, and 13 onboard NOAA 15, 16, 17, and 18 and MetOp-A are listed in Table 3. Figure 8 demonstrates the performance of these coefficients by showing their corresponding global ocean mean intersatellite difference T_b time series for channels 5, 6, 7, and 9. Figure 9 shows global ocean mean T_b difference time series between the SNO and operational calibrations for all intercalibrated NOAA 15 and NOAA 16 channels. First, as noted above, Aqua was intercalibrated in the sense that only constant offsets were obtained, because the Aqua instrument raw counts could not be easily acquired. These constant offsets were derived not through the SNO procedure, but from the global ocean differences between Aqua and the reference satellite. This

Table 3. SNO Determined Calibration Coefficients for AMSU-A Channels 4–10 and 12–13[a]

	δR_0	κ	μ_0	λ
Channel 4				
NOAA 15	0	0	−0.269	0
NOAA 16	0	0	−0.718	0
NOAA 17	0.220	0	−0.886	0
NOAA 18	0.276	0	0.929	0
MetOp-A	0.324	0	0.442	0
Aqua	−0.034			
Channel 5				
NOAA 15	0	0	0.3	0
NOAA 16	−1.846	$-7.248e^{-07}$	2.4	0
NOAA 17	0.877	0	−1.007	0
NOAA 18	0	0	1.468	0
MetOp-A	0.467	0	0.262	0
Aqua	0.023			
Channel 6				
NOAA 15	1.406	$0.614e^{-05}$	0	0.442
NOAA 16	−2.903	$-1.177e^{-06}$	4.3	0
NOAA 17	5.065	0	−3.722	0
NOAA 18	0	0	3	0
MetOp-A	1.131	0	2.389	0
Aqua	1.667			
Channel 7				
NOAA 15	0	0	0.3	0
NOAA 16	−4.475	$-3.925e^{-06}$	3.6	0
NOAA 17	3.043	0	−2.347	0
NOAA 18	1.319	0	0.479	0
MetOp-A	2.152	$-1.169e^{-06}$	0.396	0
Aqua	−0.341	0	0	0
Channel 8				
NOAA 15	0	0	0.667	0
NOAA 16	−5.043	$-1.7679e^{-06}$	4.3	0
NOAA 17	2.078	0	−1.099	0
NOAA 18	0.440	0	0.964	0
MetOp-A	1.633	0	0	0
Aqua	−0.034			
Channel 9				
NOAA 15	0	0	0.077	0
NOAA 16	−4.13	$-3.936e^{-07}$	2.3	0
NOAA 17	1.334	0	−0.809	0
NOAA 18	−0.108	0	0.820	0
MetOp-A	0.111	0	1.246	0
Aqua	−1.403			
Channel 10				
NOAA 15	0	0	0.346	0
NOAA 16	0.227	0	−0.2	0
NOAA 17	0.711	0	−0.361	0
NOAA 18	0.876	0	1.116	0
MetOp-A	0.975	0	1.148	0
Aqua	−0.189			
Channel 12				
NOAA 15	0	0	1.115	0
NOAA 16	−0.300	$-8.000e^{-07}$	1.6	0
NOAA 17	1.752	0	0	0
NOAA 18	3.390	0	0	0
MetOp-A	3.662	0	0	0
Aqua	1.754			
Channel 13				
NOAA 15	0	0	1.500	0
NOAA 16	0.702	$-8.045e^{-07}$	1.0	0
NOAA 17	1.471	0	0	0
NOAA 18	3.171	0	0	0
MetOp-A	3.018	0	0	0
Aqua	2.696			

[a]For simplicity, all δR_0 and μ_0 were adjusted to a reference time of t_0 = 2001 and t_1 = 1998. Units for δR and μ_0 are 10^{-5} (mW) (sr m^2 cm^{-1})$^{-1}$ and (sr m^2 cm^{-1}) (mW)$^{-1}$, respectively. Offset of the NOAA 15 channel 6 has been adjusted to account for its frequency shift as found in section 5. Because of unavailability of the raw counts data for Aqua, only constant offsets were obtained for this satellite.

makes Aqua being nearly identical to the reference satellites for all channels in terms of global ocean means (Figure 8). In addition, in the intersatellite bias analyses in Figures 2 and 8, no significant sun-heating-induced temperature variability were found for all Aqua channels during the time period from its launch to present. This suggests that the nonlinear calibration coefficients for Aqua AMSU-A may not need to be changed from operational values.

[44] Further analysis of Table 3 and Figures 8 and 9 suggests that the intercalibrated satellite channels can be separated into four groups:

[45] 1. Near linear channels: Most channels on NOAA 15, 17, and 18 and MetOp-A are considered as "good linear channels" when their nonlinear coefficients are smaller than about 0.5 (sr m^2 cm^{-1}) (mW)$^{-1}$, which are an order of magnitude smaller than channels with a high calibration nonlinearity. For certain channels such as NOAA 15 channels 5, 7, and 10 in this group, the SNO intercalibration generated nearly identical observations to the operational calibration as demonstrated by their nearly exact zero differences through the entire analysis period (Figure 9a). This occurs because the nonlinear coefficients in the operational calibration are similarly small (on the order of 0.1 [(sr m^2 cm^{-1}) (mW)$^{-1}$)] [see *Mo*, 1995]) as in the SNO intercalibration.

[46] Though also nearly linear, several channels (e.g., NOAA 15 channels 4, 8, and 9) show small constant differences on the order of 0.2 K between the SNO and operational calibrations. This occurred because the SNO intercalibration used a cold-space sidelobe correction different from the operational calibration. This difference affects the absolute values of the calibrated brightness temperatures and their subsequent applications in NWP and reanalysis data assimilations. Limited validation suggested that the 2 K assumption for the sidelobe effect used in this study produced AMSU-A channel 9 brightness temperatures closer to the GPS Radio Occultation (RO) observations than the operational calibrated observations (W. He, personal communication, 2011), which used 0.87 K for the cold-space sidelobe effect for this channel. Because of this, we will keep the 2 K assumption for the sidelobe effect for other channels until new evidence emerges in the future showing other assumptions could be better. Also note that the absolute values of the calibrated brightness temperatures can be easily adjusted by changing the calibration offset of the reference satellite. In this sense, choosing different values for the cold-space sidelobe effect is not a big issue. However, preliminary studies suggest that different assumptions for the sidelobe effect may affect observed patterns of the seasonal climatology. This is an emerging field and will be investigated in future studies.

[47] 2. Highly nonlinear channels: The SNO intercalibrated NOAA 15 channel 6 and most NOAA 16 channels are significantly different from its operational calibration as noted from their difference time series (Figure 9). This is expected as most NOAA 16 channels and NOAA 15 channel 6 are highly nonlinear (μ is as large as 4–5 (sr m^2 cm^{-1}) (mW)$^{-1}$ for some NOAA 16 channels and NOAA 15 channel 6 around the year 2010), and its operational calibration failed to account for them. The large nonlinear coefficients obtained from the SNO method largely removed the instrument temperature variability in NOAA 15 and NOAA 16 T_b

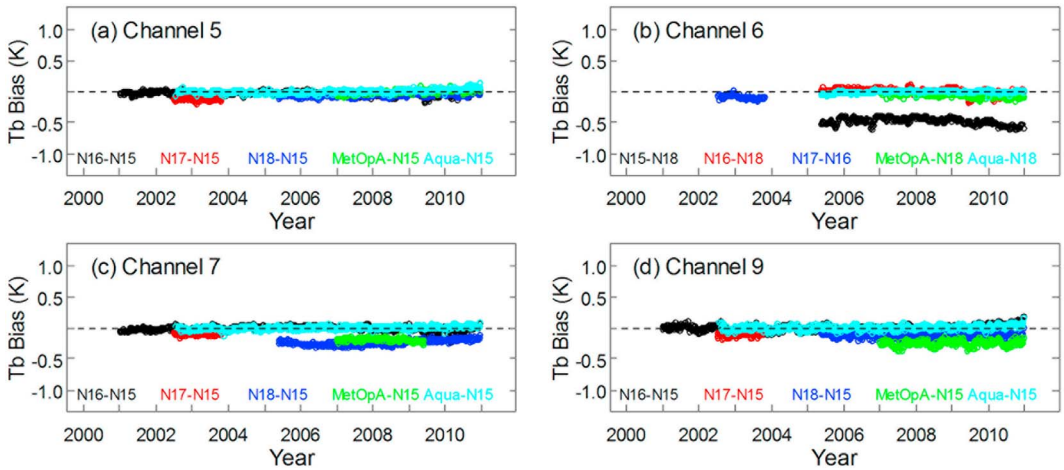

Figure 8. Same as Figure 2 except that the data are derived from SNO intercalibration. The larger biases of NOAA 15 channel 6 relative to other satellites are due to its frequency shift from the prelaunch measurement (see section 5).

observations, resulting in nearly zero intersatellite difference time series for respective satellite pairs involved in the intercalibration (Figure 8b).

[48] 3. Weakly nonlinear channels: NOAA 15 channels 12 and 13 have μ values around 1–1.5 (sr m^2 cm^{-1}) (mW)$^{-1}$. The T_b difference time series between the SNO and operational calibrations for these channels exhibit weak instrument temperature variability with magnitude much smaller than the highly nonlinear channel 6 (Figure 9a).

[49] 4. Channels with bias drifts: Nearly all NOAA 16 channels (except for channels 4 and 10) exhibit a steady bias drift before 2008 on the order of 0.2–0.5 K per decade between the SNO and operational calibrations (Figure 9b). Time-varying offsets obtained from the SNO intercalibration successfully removed the NOAA 16 bias drifts and brought their T_b values in line with the observations of other satellites for all intercalibrated channels (Figure 8).

[50] In summary, the intersatellite biases, instrument temperature variability, and bias drifts found in Figure 2 have all been significantly reduced by the SNO intersatellite calibration. For information, the biases and standard deviation of the intercalibrated difference T_b time series are typically on the order of 0.05 and 0.03 K, respectively, compared with 0.5 and 0.13 K in the operational calibration shown in Figure 2.

[51] Figure 10a shows the SNO scatterplot similar to Figure 5a between NOAA 18 and MetOp-A, demonstrating that the scene temperature dependent biases in Figure 5a have been mostly removed by the SNO intercalibration coefficients. As a result, seasonal cycles in the Arctic and Antarctic SNO time series found in Figures 5b and 5c are also significantly reduced as shown in Figures 10b and 10c. Similar results were obtained for other channels, indicating again that the calibration coefficients listed in Table 3 perform fairly well in removing respective intersatellite biases.

[52] Removal of instrument calibration errors allows the estimation of diurnal drift effect for different channels as the effect can be well isolated in the intersatellite bias analyses. Figure 11 shows global spatial bias patterns for most channels between NOAA 18 and NOAA 15 (the former minus the latter) after the SNO intercalibration. Note that NOAA 15 was a morning satellite and NOAA 18 was an afternoon satellite; their observations were roughly 6.5 hours apart at launch time. NOAA 15 then drifted for about 3 h during the analysis period (Figure 1). As such, after the calibration errors are removed, intersatellite biases can be attributed to their diurnal differences in local observation times. As shown, channels 4 and 5 have large diurnal effect over land as intersatellite biases are large over there (typically around $\pm$1 K). Over oceans, however, intersatellite biases are only around $\pm$0.1 K, indicating negligible diurnal effect for these channels. Furthermore, intersatellite biases for channels 7–10 are small ($\pm$0.1–0.2 K) over both land and oceans, suggesting negligible diurnal effect globally for these channels.

[53] Because of a frequency shift in NOAA 15 channel 6 (see section 5), intersatellite biases between NOAA 15 and NOAA 18 are too large (not shown) to draw conclusions on the diurnal effect for this channel. But from bias analysis between satellite pairs with the same channel frequency values, we found that diurnal effect for channel 6 is also negligible globally. In contrast, intersatellite biases for channels 12 and 13 are large, indicating large diurnal effect globally due to strong solar semidiurnal tides in the stratosphere.

5. Estimating Channel Frequency Shift in NOAA 15 Channel 6

[54] As shown in Figure 6, scene temperature dependent biases and seasonal cycles in the Arctic and Antarctic SNO time series between NOAA 15 and NOAA 18 still exist even when the best estimated calibration coefficients in Table 3 were applied to derive their radiances. These residual biases and SNO seasonal variability turned out to be, as seen in the following analyses, a result of a channel frequency shift in NOAA 15 channel 6. First, note that this frequency shift is not a prelaunch measurement error. To understand this, Table 4 lists the design specification as well as prelaunch measured frequencies for AMSU-A channel 6 for different NOAA and MetOp-A satellites, taken from the studies by *Mo* [1996, 2006, 2007]. It is shown that the measured frequency differences between different satellites are typically within 0.5 MHz. Our sensitivity experiments using radiative

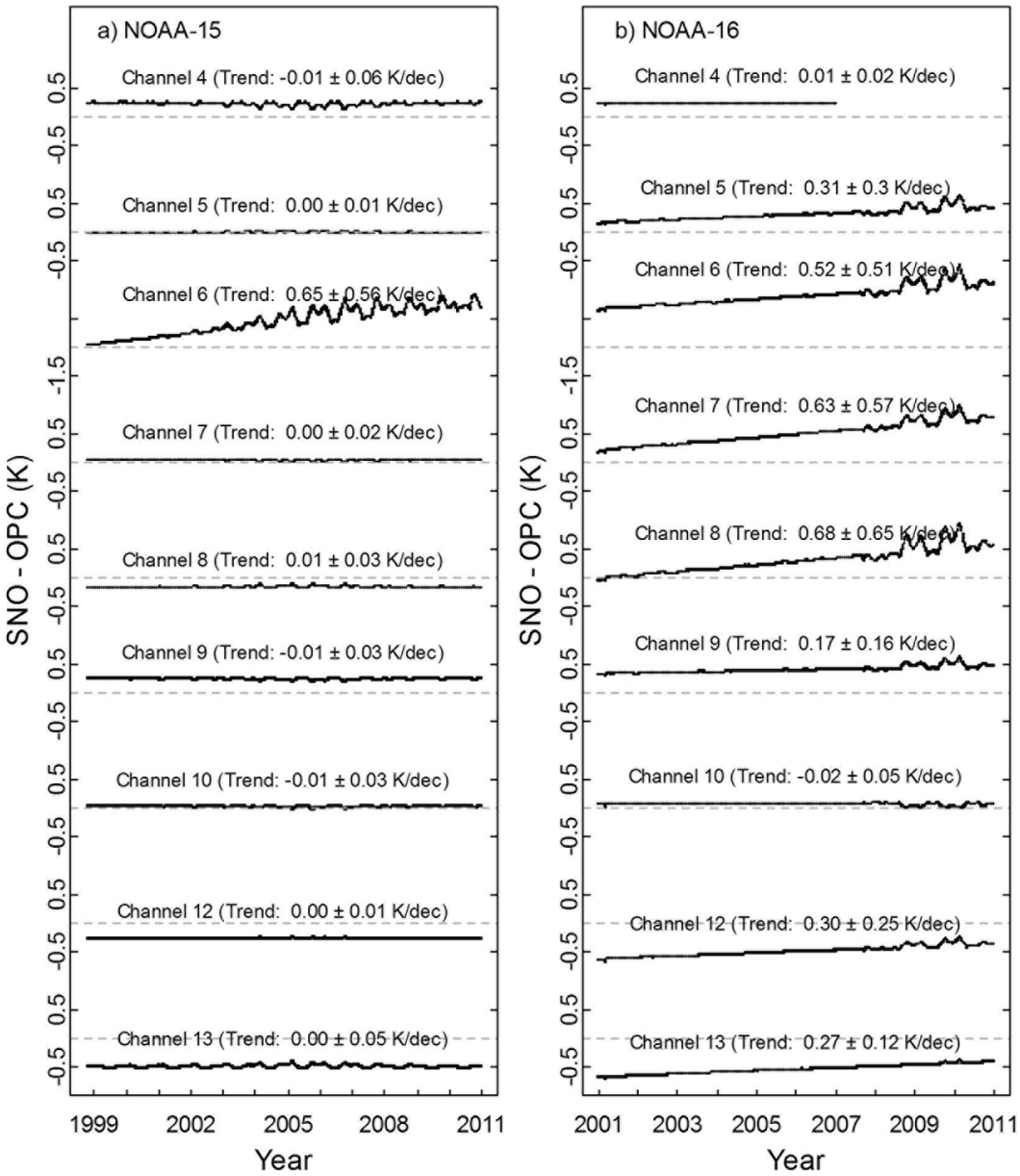

Figure 9. Global ocean mean T_b difference time series between the SNO and operational calibrations (the former minus the latter) for all intercalibrated (left) NOAA 15 and (right) NOAA 16 channels.

transfer model simulations indicated that these small differences would not produce noticeable temperature differences (actually on the order of only 0.01 K) between satellite pairs. Therefore, the measured frequencies can be considered the same for different satellites. In addition, no seasonal variability was found in the intercalibrated SNO time series between NOAA 18 and satellites other than NOAA 15 (e.g., between NOAA 18 and MetOp-A, as shown in Figure 10); thus, channel 6 frequencies of NOAA 18 and other satellites except for NOAA 15 were believed to be the same as their prelaunch measurements. NOAA 15 channel 6 frequency was thus inferred to contain a noticeable error from its prelaunch measurement, which is most likely caused by a postlaunch instrument error specific to channel 6. We suspect that this error occurred in the channel 6 local oscillator, an electronic device that determines the central channel frequency value. However, detailed information on the local oscillator is unavailable for understanding how such an error could occur.

[55] To gain further understanding of the frequency error in NOAA 15 channel 6, we simulated its observations using NOAA/Joint Center for Satellite Data Assimilation Community Radiative Transfer Model (CRTM) [*Han et al.*, 2006]. The surface temperature and atmospheric profiles including temperature, humidity, cloud liquid water, and ozone taken from NASA's MERRA reanalysis were used as inputs to the CRTM. The MERRA surface temperature is an hourly datum with a grid resolution of 0.5° latitude by 0.67°

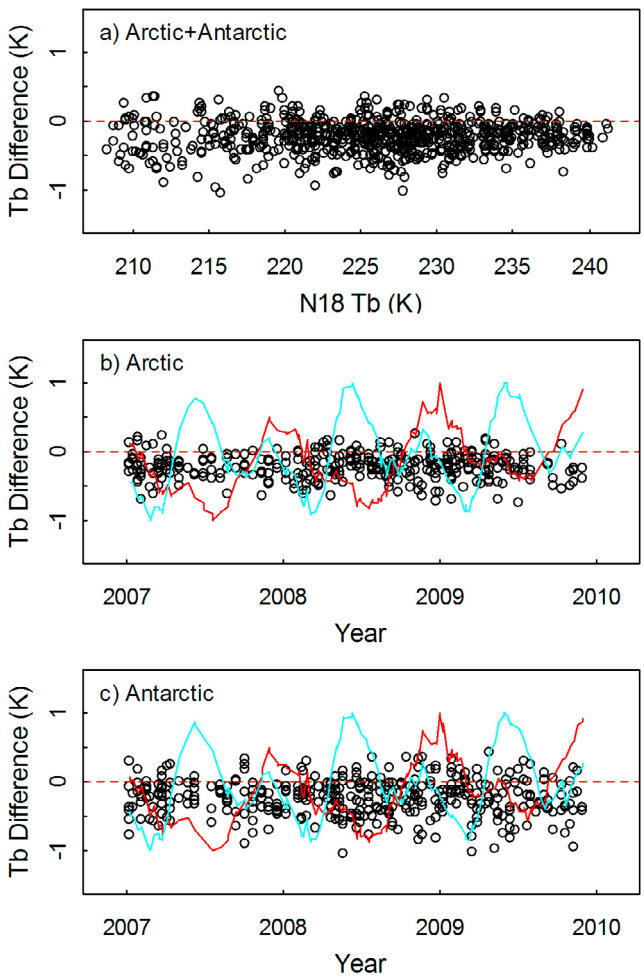

Figure 10. Same as Figure 5 except that the SNO T_b is obtained using the intercalibration coefficients listed in Table 3.

longitude. The atmospheric profiles are three hourly data with a grid resolution of 1.25° latitude by 1.25° longitude. These data were interpolated into the SNO positions and times for the NOAA 15 and NOAA 18 pair for the CRTM to generate a simulated NOAA 15 time series at these sites. Different experimental frequency values of NOAA 15 channel 6 were examined in the CRTM simulations, with its range, represented by a frequency shift, *df*, relative to its prelaunch measurement, being arbitrarily chosen from −150 to 150 MHz with an interval of 2.5 MHz.

[56] Figure 12 shows examples at $df = -40$ and 40 MHz, respectively, of the simulated NOAA 15 channel 6 T_b differences between those with prelaunch measured frequency and this measured frequency plus the shift *df*. For brevity, this T_b difference is expressed as ΔT_b^s (N15, *df*) = T_b^s (N15, $f_m + df$) − T_b^s (N15, f_m), where f_m stands for the prelaunch measured frequency, the superscript *s* stands for the simulated T_b, and N15 stands for NOAA 15. As seen, the ΔT_b^s (N15, *df*) time series exhibit seasonal variability over the Arctic and Antarctic with opposite phases. To understand this behavior, Figure 13 further shows the multiyear averaged temperature profile climatology taken from MERRA reanalysis over the Arctic (70°N) and Antarctic (70°S) for January and July, respectively. It is known that the weighting function of AMSU-A channel 6 peaks near 350 hPa for its measured frequency [*Robel*, 2009], with positive (negative) shift peaking higher (lower) in the atmosphere. Taking Antarctic as an example, the winter (July) temperature decreases throughout the atmosphere from the surface to about 10 hPa; however, the summer (January) temperature changes from decreasing vertically in the lower troposphere to increasing in the upper troposphere with a turning point occurring at about 310 hPa. This makes the averaged lapse rate around 350 hPa being steeper in winters than in summers. This lapse rate climatology translates to a ΔT_b^s (N15, *df*) time series with winter values being at the negative side of the summer values when the frequency shift is positive (weighting function peaking higher than prelaunch measured) and the other way around for the negative frequency shift. This feature happens in both hemispheres.

[57] The previous analysis is also applied to the observed SNO time series as shown in Figure 6, where the winter values of the observed T_b differences between NOAA 15 and NOAA 18, $\Delta T_b = T_b$ (N15) − T_b (N18), are at the negative side of the summer values, suggesting that the weighting function of NOAA 15 peaks higher than that of NOAA 18. In other words, the NOAA 15 channel 6 frequency should have a positive shift.

[58] To determine the actual value of the frequency shift, we examine the adjusted SNO time series, $\Delta T_b'$, between NOAA 15 and NOAA 18 in which the CRTM simulated T_b differences due to the NOAA 15 frequency shift was subtracted from the observed NOAA 15 T_b, that is,

$$\begin{aligned}\Delta T_b' &= T_b(\mathrm{N15}) - \Delta T_b^s(\mathrm{N15}, df) - T_b(\mathrm{N18}) \\ &= \left[T_b(\mathrm{N15}) - T_b^s(\mathrm{N15}, f_m + df)\right] \\ &\quad + \left[T_b^s(\mathrm{N15}, f_m) - T_b(\mathrm{N18})\right]. \end{aligned} \tag{4}$$

Minimum seasonal variability is expected as terms in the square brackets of equation (4) are expected to cancel out with each other when *df* equals to the actual frequency shift of NOAA 15 channel 6. We only examine $\Delta T_b'$ over the Antarctic because the seasonal cycle is better defined there. Figure 14 shows changes of the amplitude of the adjusted Antarctic SNO seasonal cycle, obtained by fast Fourier transform versus *df*. The amplitude of the seasonal cycle was scaled (divided) by its value at $df = 0$, so it equals 1 at $df = 0$. As seen, the amplitude of the seasonal cycle reaches 0 between $df = 35$ and 37.5 MHz. Thus, the actual frequency shift is estimated to be their average with uncertainty being half of their difference, that is, $df_o = 36.25 \pm 1.25$ MHz for NOAA 15 channel 6.

[59] Figure 15 shows the scatterplot for $\Delta T_b'$ and its time series over both the Arctic and Antarctic for the obtained frequency shift df_o. Compared to its counterpart plots, Figure 6, of the unadjusted SNO plots, the scene temperature dependent biases in Figure 6a have been mostly removed in Figure 15a, and the seasonal cycles in both Figures 6b and 6c have also been removed in Figures 15b and 15c. These results indicate that the simulated NOAA 15 T_b errors due to the frequency shift best match the observed SNO time series in both the Arctic and Antarctic at df_o. With this shift, the actual value of NOAA 15 channel 6 frequency should be 54435.73 ± 1.25 MHz (Table 4).

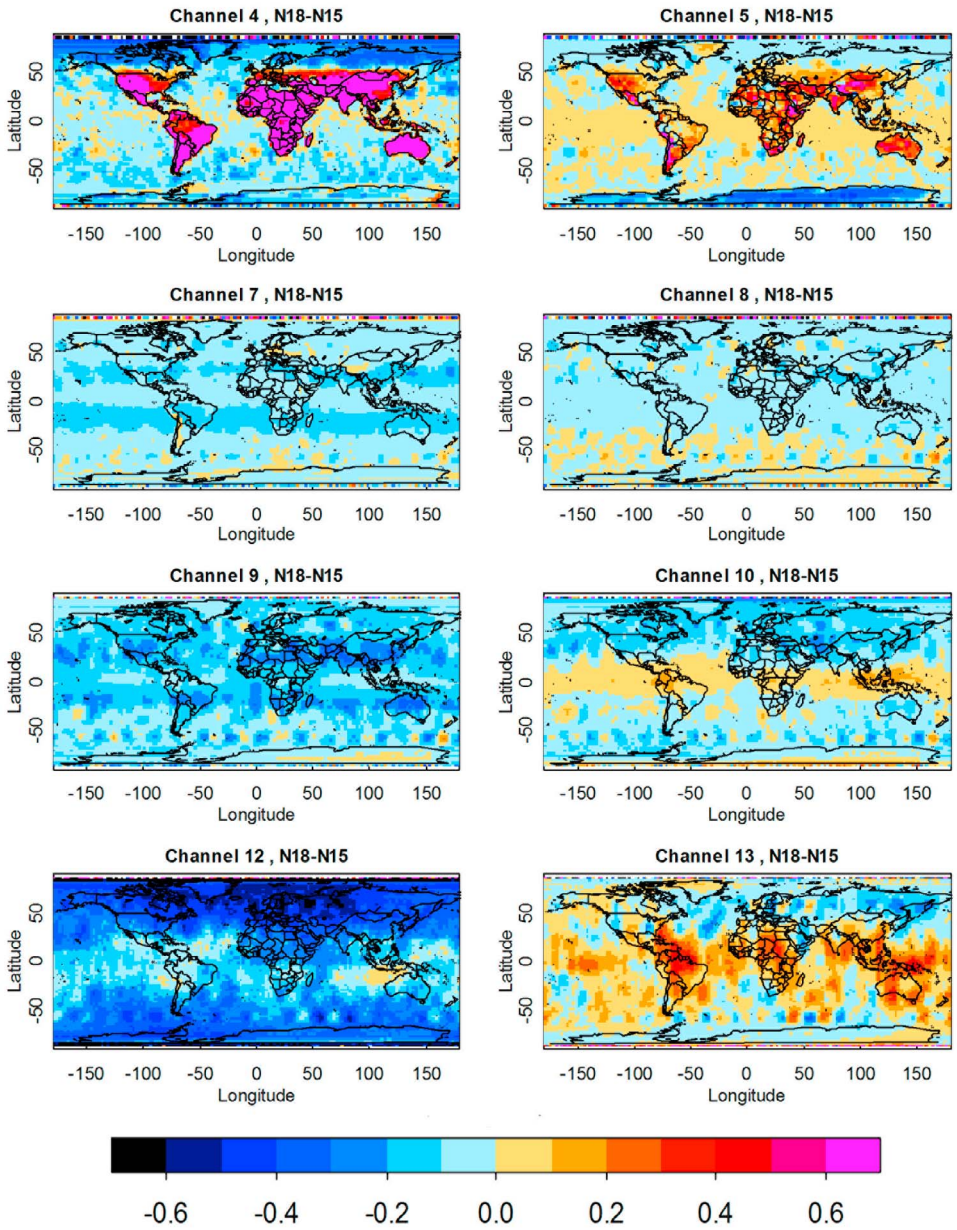

Figure 11. Spatial intersatellite bias patterns for different channels between NOAA 18 and NOAA 15 (the former minus the latter) during their overlap observations after SNO intercalibration. Units are in K.

[60] As minimization parameters used for determining *df* and μ are independent of each other, the obtained values of *df* and μ are thus independent of the orders of which procedure is conducted first. Although only NOAA 15 channel 6 frequency shift is obtained using the previous analysis method, it is expected that this method is applicable to other channels and satellites when such errors exist.

6. Merged MSU and AMSU Upper-Air Temperature Time Series

[61] A 28 year, version 1.2 MSU-only upper-air temperature time series had been developed at NOAA/STAR from the SNO intercalibrated MSU radiances. Its performance was described in earlier publications [*Zou et al.*, 2006, 2009; *Zou and Wang*, 2010]. With the availability of the AMSU-A intercalibration method, version 2.0 of a climate-quality, merged MSU/AMSU atmospheric temperature data set is further generated from the SNO intercalibrated MSU/

Table 4. Frequency Characteristics for AMSU-A Channel 6 From *Mo* [1996, 2006, 2007] and SNO Intercalibration[a]

	Measured Channel Frequency (Specification = 54,400 for All Satellites)	3 dB Bandwidth	SNO Determined Central Channel Frequency
NOAA 15	54,399.53	380.54	54,435.73 ± 1.25
NOAA 16	54,399.78	380.60	
NOAA 18	54,400.97	380.36	
MetOp-A	54,400.07	380.40	

[a]Units are in MHz.

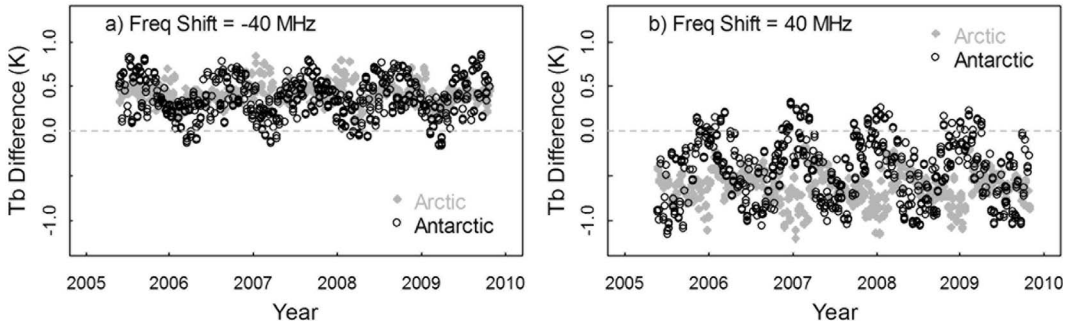

Figure 12. CRTM simulated ΔT_b^s time series for NOAA 15 channel 6 at its SNO sites relative to NOAA 18 for (a) $df = -40$ MHz and (b) $df = 40$ MHz.

AMSU level-1c radiances. This global gridded data set with 2.5° latitude by 2.5° longitude resolution is available at both monthly and pentad time resolution. Intercalibrated MSU observations from TIROS-N through NOAA 14 and AMSU-A observations from NOAA 15, 16, 17, and 18 and MetOp-A were all included in the time series. Seven near-nadir MSU footprint observations and 22 near-nadir AMSU-A footprints were used to produce the data set; here the selection of pixel numbers from the MSU and AMSU-A instruments was based on the requirement that their swath width should be similar in the merging. Note that Aqua data are not included in the STAR version 2.0 data set. However,

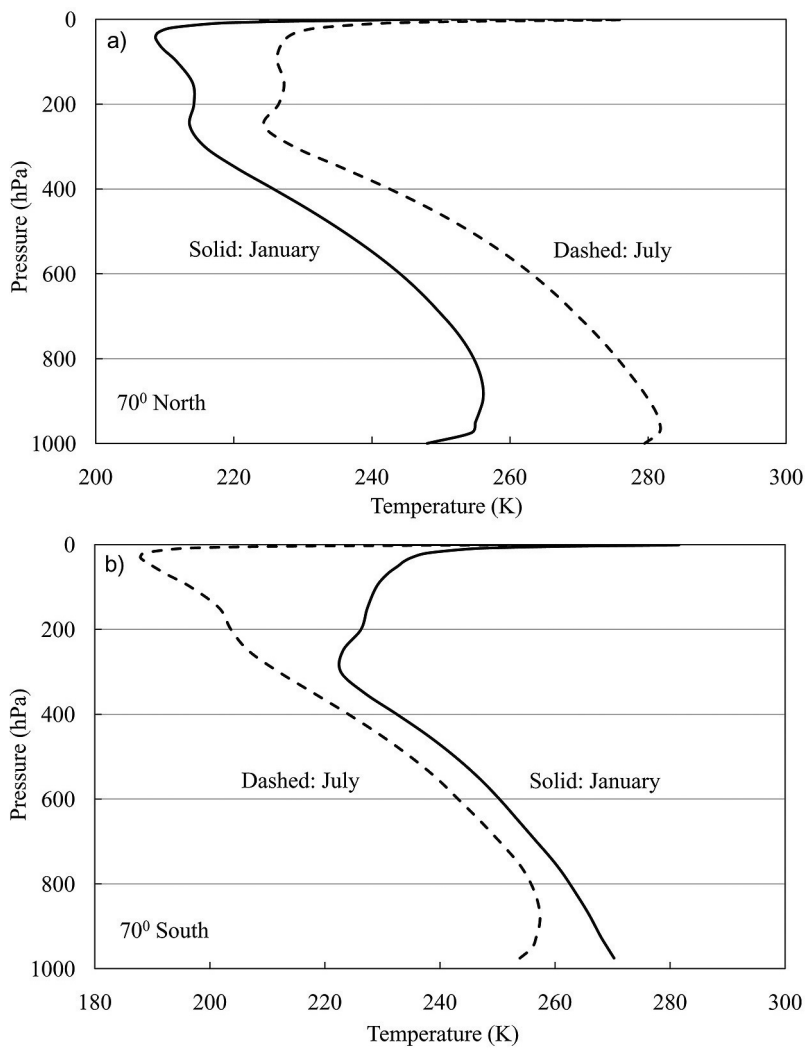

Figure 13. Temperature profile climatology from MERRA reanalysis over (a) 70°N and (b) 70°S for January and July.

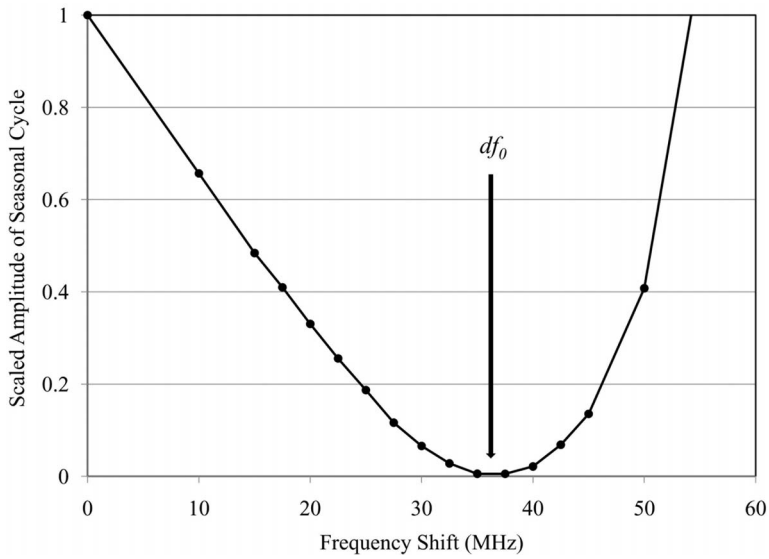

Figure 14. Amplitude of the seasonal cycles in the adjusted SNO time series over the Antarctic versus NOAA 15 channel 6 frequency shift, *df*.

because recalibrated Aqua is nearly identical to NOAA 15 (section 4), including Aqua is not expected to change the trend results as presented in the following.

[62] In addition to the SNO intercalibration to remove instrument-specific errors, several other adjustments have been made to remove errors from different sources in the time series. These include: (1) Viewing angle corrections using the limb-adjustment algorithms and coefficients developed by *Goldberg et al.* [2001], (2) diurnal drift corrections for MSU channel 2 and AMSU-A channel 5 using the diurnal anomalies developed by RSS [*Mears et al.*, 2003], (3) correction of the residual instrument temperature effect left over from the SNO intercalibration using the algorithm developed by *Christy et al.* [2000] with the correction coefficients obtained from ocean-only data, (4) removal of Earth-location dependent bias using a grid-cell-dependent constant bias correction as described by *Zou et al.* [2009] and *Zou and Wang* [2010], and (5) a bias correction to account for the frequency differences between corresponding MSU and AMSU channels. Detailed description of the first four types of bias corrections and merging procedures can be found in the studies by *Zou et al.* [2009] and *Zou and Wang* [2010] and thus skipped here. The last correction is discussed shortly in the following.

[63] The STAR version 2.0 data set offers two types of upper-air temperature TCDRs: 30+ year (1979–present) merged MSU and AMSU temperature time series using their companion channels and 13+ year (1998–present) AMSU-A only temperatures from channels that do not have the MSU equivalents. The merged MSU/AMSU time series include temperature midtroposphere (TMT, MSU channel 2 merged with AMSU-A channel 5), temperature upper troposphere (TUT, MSU channel 3 merged with AMSU-A channel 7), and temperature lower stratosphere (TLS, MSU channel 4 merged with AMSU channel 9). Figure 16 shows the monthly global mean anomaly time series for TMT, TUT, and TLS for satellites TIROS-N through NOAA 18 and MetOp-A after all intersatellite calibrations and bias

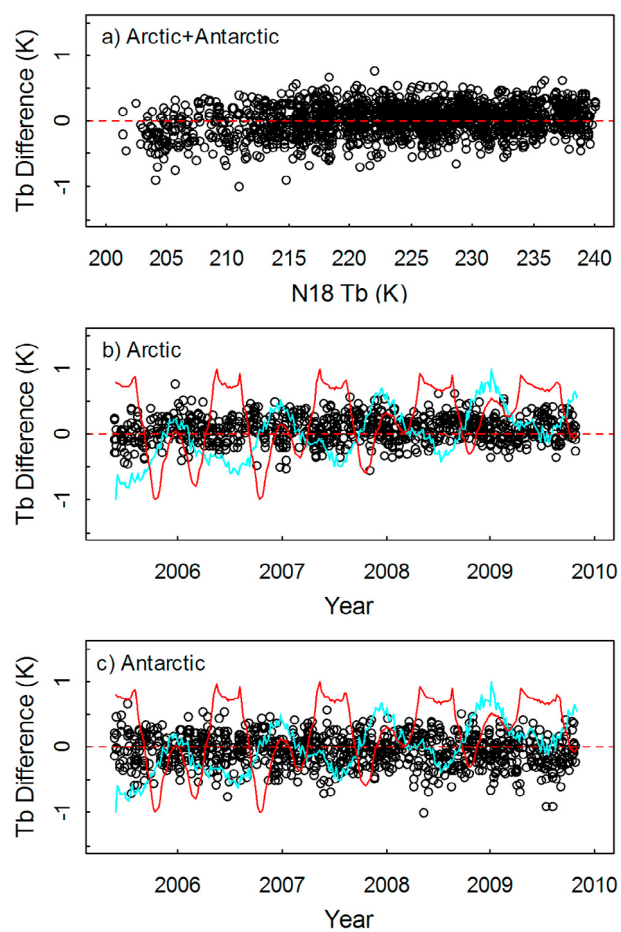

Figure 15. Same as Figure 6 except for the adjusted SNO time series, $\Delta T_b'$, between NOAA 15 and NOAA 18 in which the CRTM simulated differences due to the NOAA 15 frequency shift was subtracted from the observed NOAA 15 T_b.

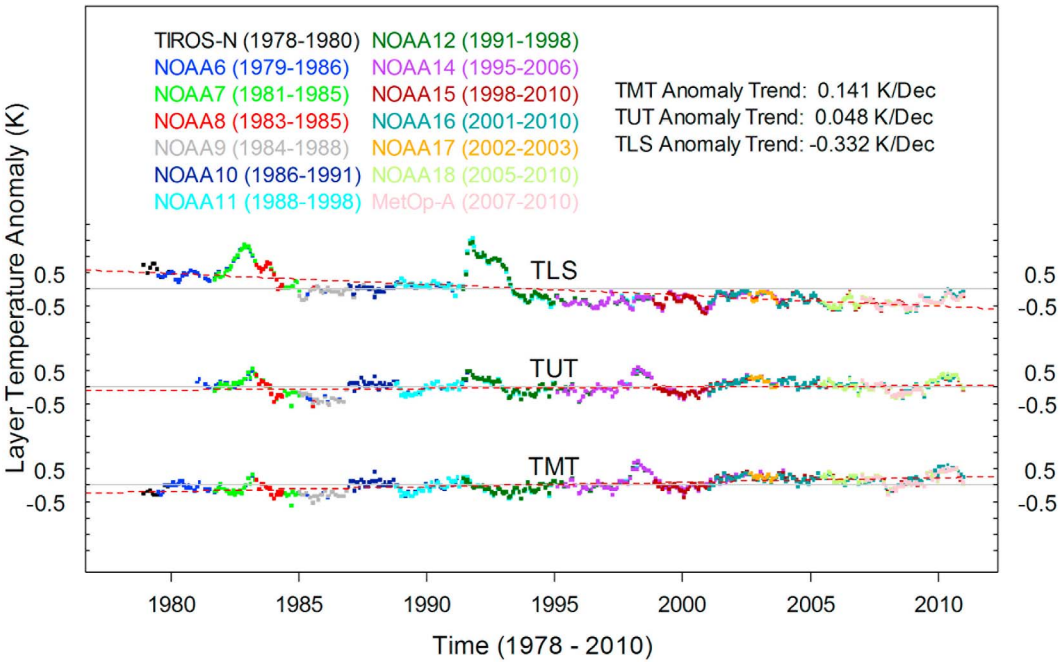

Figure 16. STAR version 2.0 of the monthly global mean anomaly time series for satellites TIROS-N through NOAA 18 and MetOp-A for TMT, TUT, and TLS after all intercalibration and bias corrections were made. Time series of different colors represent different satellites. The red dashed lines are least squares linear trend lines for the time series.

corrections were made. As seen, different satellites agree with each other on a point-by-point basis during overlapping observations, and no obvious relative drifts exist between any satellite pairs. This indicates the excellent performance of the intersatellite calibration and bias correction algorithms applied to the data set.

[64] A single time series was obtained by averaging the available bias-corrected multisatellite observations at any point, and climate trend was further computed from the single time series. As shown in the plot, the global mean trends from 1979 to 2010 for TMT and TLS are 0.141 and −0.332 K per decade, respectively, and the TUT trend from 1981 to 2010 is 0.048 K per decade.

[65] It is desirable to understand the bias corrections between the MSU and AMSU-A equivalent channels. The level-1c AMSU-A intercalibration presented in this study and the MSU intercalibration in our previous studies [*Zou et al.*, 2006, 2009] were carried out independently from each other. Because of the frequency differences, the MSU and AMSU-A equivalent channels exhibit seasonally dependent intersatellite biases, similar to AMSU-A channel 6 between NOAA 15 and NOAA 18 as found in the previous sections. The patterns of these seasonally dependent biases may depend on geographic locations and channels, because lapse rate climatology is a function of atmospheric locations. To reduce this type of biases, yearly mean monthly (pentad) bias statistics between MSU and AMSU-A are derived for each of their equivalent channels and grid cells. These biases are then subtracted from the monthly (pentad) AMSU-A data, so that they become MSU equivalent channel observations. The effect of this step, along with other bias correction procedures, as mentioned earlier, is demonstrated in Figure 17 with the global mean difference time series of TMT, TUT, and TLS between version 1.2 MSU-only and version 2.0 merged MSU/AMSU data records. It is shown that over the period from 1979 to 1997, when only MSU observations were available, versions 1.2 and 2.0 data are nearly identical for all TMT, TUT, and TLS, suggesting consistencies in version transitions. Over the period of 1998 to 2003, version 2.0 included both MSU and AMSU-A observations, but version 1.2 only had NOAA 14 MSU observations. No significant seasonally dependent biases are found between versions 1.2 and 2.0 for global means over this period. One reason for this is that the seasonally dependent bias corrections have reduced such errors to some extent in the version 2.0 data record. The other reason is that global means are dominated by the tropical atmosphere where lapse rate has less seasonal variations, especially in the troposphere [e.g., *Stone and Carlson*, 1979]. Over the middle and high latitudes, difference time series between versions 1.2 and 2.0 data show seasonally dependent biases with larger magnitudes for all TMT, TUT, and TLS (not shown). In this sense, more accurate adjustments need to be developed to remove seasonally dependent biases due to frequency differences between MSU and AMSU-A equivalent channels. This issue will be further addressed in future studies when versions of the MSU/AMSU temperature data record are upgraded.

[66] Also shown in Figure 17, the global mean trend differences between versions 1.2 and 2.0 are near zero for 1979–2003 for all TMT, TUT, and TLS. However, starting from early 2004, NOAA-14 MSU drifted away from the intercalibrated AMSU-A observations. Because of this, the

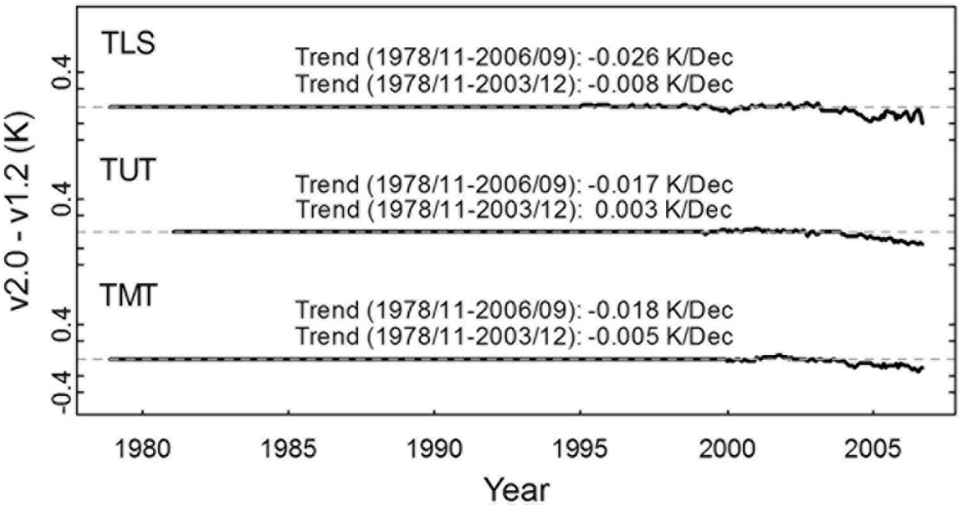

Figure 17. Global mean difference time series for TMT, TUT, and TLS between overlapping STAR version 1.2 MSU-only and version 2.0 merged MSU/AMSU data records.

version 2.0 data do not include MSU observations after December 2003. As a result, the version 2.0 trends are found cooler than version 1.2 for about 0.017 K per decade for TMT and TUT and 0.026 K per decade for TLS over the period of 1979–2006.

7. Summary

[67] Long-term observations from the AMSU-A sounding channels onboard polar-orbiting satellites NOAA 15, 16, 17 and 18; MetOp-A; and Aqua were intercalibrated using their overlap observations. Five different types of biases were identified in existing operational calibrated AMSU-A observations that need to be removed or minimized in the intercalibration processes. These included stable intersatellite biases between most satellite pairs, bias drifts on NOAA 16 and MetOp-A channel 7, instrument temperature variability in NOAA 15 channel 6 and NOAA 16 radiances, scene temperature dependency in biases due to inaccurate calibration nonlinearity, and biases due to channel frequency shift from its prelaunch measurement in NOAA 15 channel 6.

[68] A two-point level-1c quadratic nonlinear calibration equation was used to convert the AMSU-A raw counts data into radiances, and time-dependent calibration coefficients were introduced to remove or minimize bias drifts and nonlinear errors. The calibration coefficients, including calibration offsets and nonlinear coefficients, were determined from SNO regressions with a strong constraint that the sun-heating-induced instrument temperature variability should be minimized for all satellite pairs being intercalibrated. New calibration coefficients, which are different from those obtained from the operational calibration, were determined from the procedure for the intercalibrated satellites. Only constant intersatellite offsets were obtained for Aqua because its raw counts data are not easily acquired. For channels having near linear calibration characteristics, the SNO method produced a recalibrated radiance data set similar to the operational calibration except for different calibration offsets. For channels with the high calibration nonlinearity or bias drifts, the SNO method significantly reduced these time-varying biases that existed in the operational calibration. The intercalibration resulted in more consistent multisatellite radiance observations for all respective channels. A spatial bias pattern analysis of the intercalibrated observations also showed that diurnal effects are negligible over oceans for AMSU-A channels 4 and 5 and globally for channels 6–10.

[69] The channel frequency shift in NOAA 15 channel 6 was determined from CRTM model simulation experiments. Nonuniform scatter and temporal patterns in intersatellite biases associated with the frequency shift were mostly removed by the corrected channel frequency value, indicating that the methodology for determining the frequency shift is robust. The method is expected to be applicable to other channel or instrument observations with the similar error sources. In summary, the intercalibration procedure has removed or minimized all five different types of calibration errors identified in the operational calibration.

[70] STAR version 2.0 upper-air temperature CDR was generated from the SNO intercalibrated MSU/AMSU-A level-1c radiances onboard TIROS-N through NOAA 18 and MetOp-A. The data set includes monthly and pentad global MSU/AMSU-A time series of TMT, TUT, and TLS from 1979 to present with a grid resolution of 2.5° latitude by 2.5° longitude. The data sets also include AMSU-only upper-air temperature time series from 1998 to present for channels without MSU equivalents. The STAR version 2.0 monthly gridded data set is updated every month. Each update will add the monthly mean, intercalibrated, and multisatellite merged AMSU-A observations from the last month to the data set. This allows up-to-date monitoring of the upper-air temperature changes on a routine basis. The intercalibrated MSU and AMSU-A radiances and their merged temperature time series are both available at the STAR website, http://www.orbit.nesdis.noaa.gov/smcd/emb/mscat/mscatmain.htm.

[71] Currently, most NWP models and climate reanalyses use operational calibrated AMSU-A radiances as input in their data assimilation systems with a bias correction applied to the satellite data for them to be consistent with model

simulations and other observations. With intersatellite biases largely removed, the intercalibrated AMSU-A radiances are expected to further improve NWP forecasting skills and consistent climate reanalysis development where accurate channel frequencies and consistent input data sets with biases as small as possible are required. Although intersatellite biases have been mostly removed, however, the absolute value of the intercalibrated AMSU-A brightness temperature has not been adjusted to an absolute truth. This is because the calibration offset of the reference satellite was arbitrarily assumed to be zero. This assumption does not affect the intersatellite calibration nor the variability and trend analysis of the merged satellite temperature products. However, it affects the radiance applications that would consider these observations as absolute references, for example, for satellite retrieval and NWP and modeling reanalysis data assimilations. To facilitate these applications, this unknown offset for each channel needs to be determined in a validation process of satellite data against certain reference observations, ideally SI-traceable standards. Unfortunately, SI-traceable standards for the microwave instrument are currently unavailable. Other plans for such a validation are being developed at NOAA/National Environmental Satellite, Data, and Information Service (NESDIS) as part of the effort for satellite recalibration. This includes comparisons against GPS RO observations as well as observations from the Global Climate Observing System Upper-Air Network. However, because all observations feature certain errors, there is no guarantee that such comparisons will result in the offset values with required accuracies. Ultimately, community consensus references for absolute calibration need to be developed, which still remains a challenging task.

[72] **Acknowledgments.** The authors thank Tom Kleespies for providing the code for the Solar Beta Angle computation. The authors also thank Yong Han and Yong Chen for providing CRTM training data sets for related computations. Review comments from Jerry Sullivan, Paul Poli, and the three anonymous reviewers are greatly appreciated. The work is supported by NOAA grant NESDIS-NESDISPO-2009-2001589 (SDS-09-15). The views, opinions, and findings contained in this report are those of the authors and should not be construed as an official National Oceanic and Atmospheric Administration or U.S. Government position, policy, or decision.

References

Cao, C., M. Weinreb, and H. Xu (2004), Predicting simultaneous nadir overpasses among polar-orbiting meteorological satellites for the intersatellite calibration of radiometers, *J. Atmos. Oceanic Technol.*, *21*, 537–542, doi:10.1175/1520-0426(2004)021<0537:PSNOAP>2.0.CO;2.

Cao, C., H. Xu, J. Sullivan, L. McMillin, P. Ciren, and Y.-T. Hou (2005), Intersatellite radiance biases for the high-resolution infrared radiation sounders (HIRS) on board NOAA 15, 16, and 17 from simultaneous nadir observations, *J. Atmos. Oceanic Technol.*, *22*, 381–395, doi:10.1175/JTECH1713.1.

Christy, J. R., R. W. Spencer, and W. D. Braswell (2000), MSU tropospheric temperatures: Data set construction and radiosonde comparisons, *J. Atmos. Oceanic Technol.*, *17*, 1153–1170, doi:10.1175/1520-0426(2000)017<1153:MTTDCA>2.0.CO;2.

Christy, J. R., R. W. Spencer, W. B. Norris, and W. D. Braswell (2003), Error estimates of version 5.0 of MSU-AMSU bulk atmospheric temperature, *J. Atmos. Oceanic Technol.*, *20*, 613–629, doi:10.1175/1520-0426(2003)20<613:EEOVOM>2.0.CO;2.

Dee, D., and S. Uppala (2009), Variational bias correction of satellite radiance data in the ERA-Interim reanalysis, *Q. J. R. Meteorol. Soc.*, *135*, 1830–1841, doi:10.1002/qj.493.

Derber, J. C., and W.-S. Wu (1998), The use of TOVS cloud-cleared radiances in the NCEP SSI analysis system, *Mon. Weather Rev.*, *126*, 2287–2299, doi:10.1175/1520-0493(1998)126<2287:TUOTCC>2.0.CO;2.

English, S. J., R. J. Renshaw, P. C. Dibben, A. J. Smith, P. J. Rayer, C. Poulsen, F. W. Saunders, and J. R. Eyre (2000), A comparison of the impact of TOVS and ATOVS satellite sounding data on the accuracy of numerical weather forecasts, *Q. J. R. Meteorol. Soc.*, *126*, 2911–2931.

Goldberg, M., et al. (2011), The Global Space-Based Inter-Calibration System, *Bull. Am. Meteorol. Soc.*, *92*, 467–475, doi:10.1175/2010BAMS2967.1.

Goldberg, M. D., D. S. Crosby, and L. Zhou (2001), The limb adjustment of AMSU-A observations: Methodology and validation, *J. Appl. Meteorol.*, *40*, 70–83, doi:10.1175/1520-0450(2001)040<0070:TLAOAA>2.0.CO;2.

Han Y., P. van Delst, Q. Liu, F. Weng, B. Yan, R. Treadon, and J. Derber (2006), JCSDA community radiative transfer model (CRTM)–Version 1, *NOAA Tech. Rep. NESDIS 122*, 40 pp., Natl. Oceanic and Atmos. Admin., Silver Spring, Md.

Iacovazzi, R. A., C. Cao, and S.-A. Boukabara (2009), Analysis of polar-orbiting operational environmental satellite NOAA-14 MSU and NOAA-15 AMSU-A relative measurement biases for climate change detection, *J. Geophys. Res.*, *114*, D09107, doi:10.1029/2008JD011588.

Mears, C. A., and F. J. Wentz (2009), Construction of the Remote Sensing Systems V3.2 atmospheric temperature records from the MSU and AMSU microwave sounders, *J. Atmos. Oceanic Technol.*, *26*, 1040–1056, doi:10.1175/2008JTECHA1176.1.

Mears, C. A., M. C. Schabel, and F. J. Wentz (2003), A reanalysis of the MSU channel 2 tropospheric temperature record, *J. Clim.*, *16*, 3650–3664, doi:10.1175/1520-0442(2003)016<3650:AROTMC>2.0.CO;2.

Mo, T. (1995), A study of the microwave sounding unit on the NOAA-12 satellite. *IEEE Trans. Geosci. Remote Sens.*, *33*, 1141–1152.

Mo, T. (1996), Prelaunch calibration of the advanced microwave sounding unit-A for NOAA-K, *IEEE Trans. Microwave Theory Tech.*, *44*, 1460–1469.

Mo, T. (1999), AMSU-A antenna pattern corrections, *IEEE Trans. Geosci. Remote Sens.*, *37*, 103–112, doi:10.1109/36.739131.

Mo, T. (2006), Calibration of the advanced microwave sounding unit-A radiometer for METOP-A, *NOAA Tech. Rep. NESDIS 121*, Natl. Oceanic and Atmos. Admin., Silver Spring, Md.

Mo, T. (2007), Postlaunch calibration of the NOAA-18 advanced microwave sounding unit-A, *IEEE Trans. Geosci. Remote Sens.*, *45*, 1928–1937.

Rienecker, M. M., et al. (2011), MERRA: NASA's Modern-Era Retrospective Analysis for Research and Applications, *J. Clim.*, *24*, 3624–3648, doi:10.1175/JCLI-D-11-00015.1.

Robel, J. (Ed.) (2009), NOAA KLM user's guide, 2009 revision, Natl. Oceanic and Atmos. Admin., Silver Spring, Md. (Available at http://www.ncdc.noaa.gov/oa/pod-guide/ncdc/docs/klm/cover.htm.)

Saha, S., et al. (2010), The NCEP climate forecast system reanalysis, *Bull. Am. Meteorol. Soc.*, *91*, 1015–1057, doi:10.1175/2010BAMS3001.1.

Spencer, R. W., and J. R. Christy (1992), Precision and radiosonde validation of satellite gridpoint temperature anomalies. Part I: MSU Channel 2, *J. Clim.*, *5*, 847–857, doi:10.1175/1520-0442(1992)005<0847:PARVOS>2.0.CO;2.

Stone, P. H., and J. H. Carlson (1979), Atmospheric lapse rate regimes and their parameterization, *J. Atmos. Sci.*, *36*, 415–423, doi:10.1175/1520-0469(1979)036<0415:ALRRAT>2.0.CO;2.

Twarog, E. M., W. E. Purdy, P. W. Gaiser, K. H. Cheung, and B. E. Kelm (2006), WindSat on-orbit warm load calibration, *IEEE Trans. Geosci. Remote Sens.*, *44*, 516–529, doi:10.1109/TGRS.2005.863300.

Zou, C.-Z., and W. Wang (2010), Stability of the MSU-derived atmospheric temperature trend, *J. Atmos. Oceanic Technol.*, *27*, 1960–1971, doi:10.1175/2009JTECHA1333.1.

Zou, C.-Z., M. Goldberg, Z. Cheng, N. Grody, J. Sullivan, C. Cao, and D. Tarpley (2006), Recalibration of microwave sounding unit for climate studies using simultaneous nadir overpasses, *J. Geophys. Res.*, *111*, D19114, doi:10.1029/2005JD006798.

Zou, C.-Z., M. Gao, and M. Goldberg (2009), Error structure and atmospheric temperature trends in observations from the Microwave sounding Unit, *J. Clim.*, *22*, 1661–1681, doi:10.1175/2008JCLI2233.1.

W. Wang and C.-Z. Zou, Center for Satellite Applications and Research, NESDIS, NOAA, NOAA Science Center, Room 712, 5200 Auth Rd., Camp Springs, MD 20746, USA. (cheng-zhi.zou@noaa.gov)